MICROCOPY RESOLUTION TEST CHART

NATIONAL BUREAU OF STANDARDS-1963-A

$E\ 301864$

(12)

ADAPTIVE ANTENNA NULLING PERFORMANCE IN A DISPERSIVE PROPAGATION MEDIUM

Ronald Y. Ibaraki
Ernest T. Tsui
MAXIM Technologies, Inc.
3930 Freedom Circle, Suite A
Santa Clara, CA 95054

15 February 1985

Technical Report

DTIC
ELECTE
DEC 19 1985
S   D
B

Prepared for
    Director
    DEFENSE NUCLEAR AGENCY
    Washington, DC 20305-1000

REPORT DOCUMENTATION PAGE

1a. REPORT SECURITY CLASSIFICATION UNCLASSIFIED	1b. RESTRICTIVE MARKINGS
2a. SECURITY CLASSIFICATION AUTHORITY	3. DISTRIBUTION/AVAILABILITY OF REPORT Approved for public release; distribution is unlimited.
2b. DECLASSIFICATION/DOWNGRADING SCHEDULE N/A since UNCLASSIFIED	

4. PERFORMING ORGANIZATION REPORT NUMBER(S) MT-TR-8502S	5. MONITORING ORGANIZATION REPORT NUMBER(S) DNA-TR-85-75

6a. NAME OF PERFORMING ORGANIZATION MAXIM Technologies, Inc.	6b. OFFICE SYMBOL (If applicable)	7a. NAME OF MONITORING ORGANIZATION Director Defense Nuclear Agency
6c. ADDRESS (City, State, and ZIP Code) 3930 Freedom Circle, Suite A Santa Clara, CA 95054		7b. ADDRESS (City, State, and ZIP Code) Washington, DC 20305-1000

8a. NAME OF FUNDING/SPONSORING ORGANIZATION	8b. OFFICE SYMBOL (If applicable)	9. PROCUREMENT INSTRUMENT IDENTIFICATION NUMBER DNA 001-83-C-0321

8c. ADDRESS (City, State, and ZIP Code)	10. SOURCE OF FUNDING NUMBERS			
	PROGRAM ELEMENT NO.	PROJECT NO.	TASK NO.	WORK UNIT ACCESSION NO.
	62715H	X99QMXV	E	DH007180

11. TITLE (Include Security Classification)

ADAPTIVE ANTENNA NULLING PERFORMANCE IN A DISPERSIVE PROPAGATION MEDIUM

12. PERSONAL AUTHOR(S)
Ibaraki, Ronald Y., Tsui, Ernest T.

13a. TYPE OF REPORT Technical Report	13b. TIME COVERED FROM 830915 TO 850115	14. DATE OF REPORT (Year, Month, Day) 850215	15. PAGE COUNT 58

17	COSATI CODES		18 SUBJECT TERMS (Continue on reverse if necessary and identify by block number)
FIELD	GROUP	SUB-GROUP	Scintillations Phased Arrays
22	02		Striations Antijam
17	02		Fading Adaptive Nulling Antennas

19. ABSTRACT (Continue on reverse if necessary and identify by block number)

The Signal-to-Interference plus Noise Ratio (SINR) performance of a generic Multi-Beam Antenna (MBA) and a Thinned Phased Array Antenna (TPAA) is evaluated for multiple jammer scenarios including the effect of angle-of-arrival distortion of the jamming signals caused by a striated propagation media. The analysis is based on computer modeling of the antenna configurations using the optimal Wiener solution for the adaptive weight calculations. Statistically distributed SINR values in fading are obtained by applying the equivalent effect of independent two-dimensional sample functions of spatially varying flat fading at the antenna aperture.

20. DISTRIBUTION/AVAILABILITY OF ABSTRACT ☐ UNCLASSIFIED/UNLIMITED ☒ SAME AS RPT ☐ DTIC USERS	21. ABSTRACT SECURITY CLASSIFICATION UNCLASSIFIED
22a. NAME OF RESPONSIBLE INDIVIDUAL Betty L. Fox	22b. TELEPHONE (Include Area Code) (202)325-7042 22c. OFFICE SYMBOL DNA/STTI

DD FORM 1473, 84 MAR   83 APR edition may be used until exhausted.   SECURITY CLASSIFICATION OF THIS PAGE
                                  All other editions are obsolete.

18.   SUBJECT TERMS (Continued)

      Multi-Beam Antenna (MBA)

SUMMARY

A set of computer programs were written to model the antijam
performance of two generic adaptive nulling antenna
configurations against jamming signals which have propagated
through spatially dispersive fading media. The two antenna
configurations examined are the MBA and TPAA configurations.
The channel effects were modeled with simulated two-dimensional
flat fading sample functions having the specified radial
decorrelation lengths.

Performance evaluations are based on the fully adapted
steady-state optimal Wiener weight solution. The effect of the
spatially fading media is modeled as a 2-D multiplicative
decorrelation term across the aperture of the nulling antenna.

The plane wavefront from a single point signal source
is scattered by the propagation media to make the source appear
as if it is many lower-power, spatially distributed, time-
varying, correlated signal sources. Null forming on many lower
power jamming sources is generally less effective than nulling
a single strong jamming source. In addition, the angular
scintillation affects gain in the direction of the desired
signal. The loss of nulling effectiveness together with
variation in desired signal will cause variations in the
received SINR. At the antenna, the angular scattering
manifests itself as random amplitude and phase variations
across the aperture. Note that in this study, all jammers are
identically faded, and the signal may or may not be fading.

i

The fading-caused variations will degrade SINR in some instances and also improve SINR in others. Average SINR loss is not an adequate measure of communication system performance, but must be complemented with the actual fading SINR density or loss distribution to more accurately characterize performance.

The results obtained in this computer aided analysis show that fading-caused loss of spatial coherence at the adaptive nulling antenna can cause several dB additional loss in SINR when the decorrelation length of the channel at the receiving antenna is of the order of the aperture diameter. The actual loss numbers, however, are highly dependent on the specific antenna type, singlet (single element) beamwidths, look angles, coverage pattern, and jamming scenario.

In general, the SINR loss is more pronounced for narrower beamwidth antennas like the TPAA whose nulling beamwidths are also much narrower than the broad area coverage pattern and broad nulls of the MBA. This result agrees with the fact that TPAA nulling is heavily dependent on phase coherence across the array using phase shifts of the identically directed antenna cluster elements to form nulls, while MBA nulling is less phase dependent and more dependent on switching off beams directed toward the jammer to form its nulls.

The TPAA case showed significant SINR phase decorrelation loss variation with increasing angular scattering (increasing stress level) when all jammers and the desired signal were identically fading, but very little loss variation when only the jammers were fading. In contrast, for the MBA case, there was very little loss variation when all jammers and the desired signal were fading, but the loss variation became noticable when only the jammers were fading. In all cases, significant loss occurs only a small percentage of the time.

It was conjectured that the use of fixed precomputed non-adaptive weights would be worse in SINR performance than weights that were adaptively recomputed as the channel caused phase variations across the aperture varied. However, for the MBA case with all jammers and desired signal identically fading it was found that the non-adaptive weights actually provided better SINR performance than the adaptive weights.

iii

TABLE OF CONTENTS

LIST OF ILLUSTRATIONS

LIST OF ILLUSTRATIONS (Continued)

SECTION 1

INTRODUCTION

1.1 INTRODUCTION

The ever increasing mobile electronic countermeasures
(ECM) jamming threat has led to increasing use of adaptive
nulling antennas to meet the requirement for secure, antijam
satellite communications. With proper design, nulling antennas
can add many more dB of jam resistance to system performance in
addition to that already provided by spread spectrum processing
techniques.

Ionospheric striations are known to cause angular
scattering of signals propagating through them[1]. The purpose
of this study is to determine what effect the angle-of-arrival
distribution of point jamming sources will have on the nulling
capabilities of adaptive null forming antenna systems. A
second, but no less important objective, is to understand the
mechanism by which any degradation occurs so that methods of
minimizing its effects can be developed.

A jamming signal propagating through a striated media is
scattered and results in a distortion of the angle-of-arrival
of the jamming signal emerging from the media. The severity of
this distortion at the receiving antenna is a function of the
strength and spatial extent of the media, the carrier
frequency, the beamwidth of the transmitting antenna, as well
as the distance of the media from both the transmitting and
receiving antennas of interest.

1

Figure 1 shows conceptually the interrelationships between all these parameters and how the dispersive media gives rise to the spatially distributed jamming effect as well as angular coherence loss. Normally, signals in free space propagate in a straight line of sight path from transmitter to receiver. The received signal power is calculated using the conventional 1/r2 loss formula. When a dispersive media interdicts this propagation path, however, angular scattering of the incident jamming rays will cause jamming energy to be received from angular directions other than the direct path, while the energy in the direct path is reduced.

Coherence loss, also shown in this figure, occurs when the angular selectivity of either the transmitting or receiving antenna prevents the reception of scattered signal energy from wide angles that could be supported by the media. The reciprocal nature of this effect is also shown in Figure 2.

1.2 OVERVIEW

The approach used in this study is based on computer modeling of generic antenna configurations which were subjected to angle-of-arrival channel distortion sample functions, in contrast to the analytical approach to the problem used by Bello[2]. The first step was to develop suitable generic models of representative nulling antennas. The two antenna types of interest that were evaluated are a Multi-Beam Antenna (MBA) and a Thinned Phased Array Antenna (TPAA). As a first cut analysis, it was decided to evaluate steady-state nulling performance using the optimal Wiener solution for antenna weight calculations. This choice is appropriate since many of the adaptive algorithms converge to this solution[3]. These
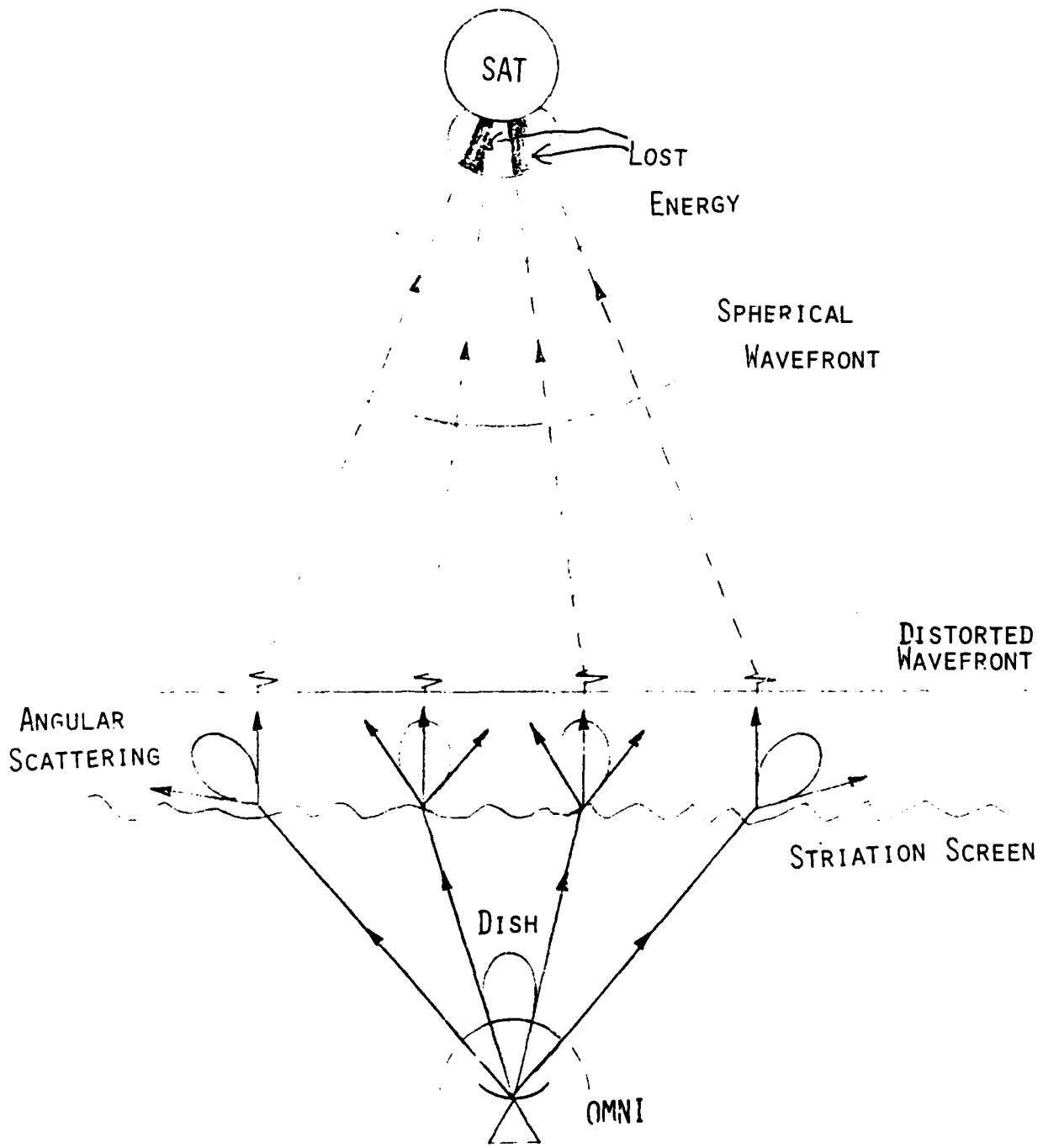
Figure 1. Uplink Distributed Jamming Effect.
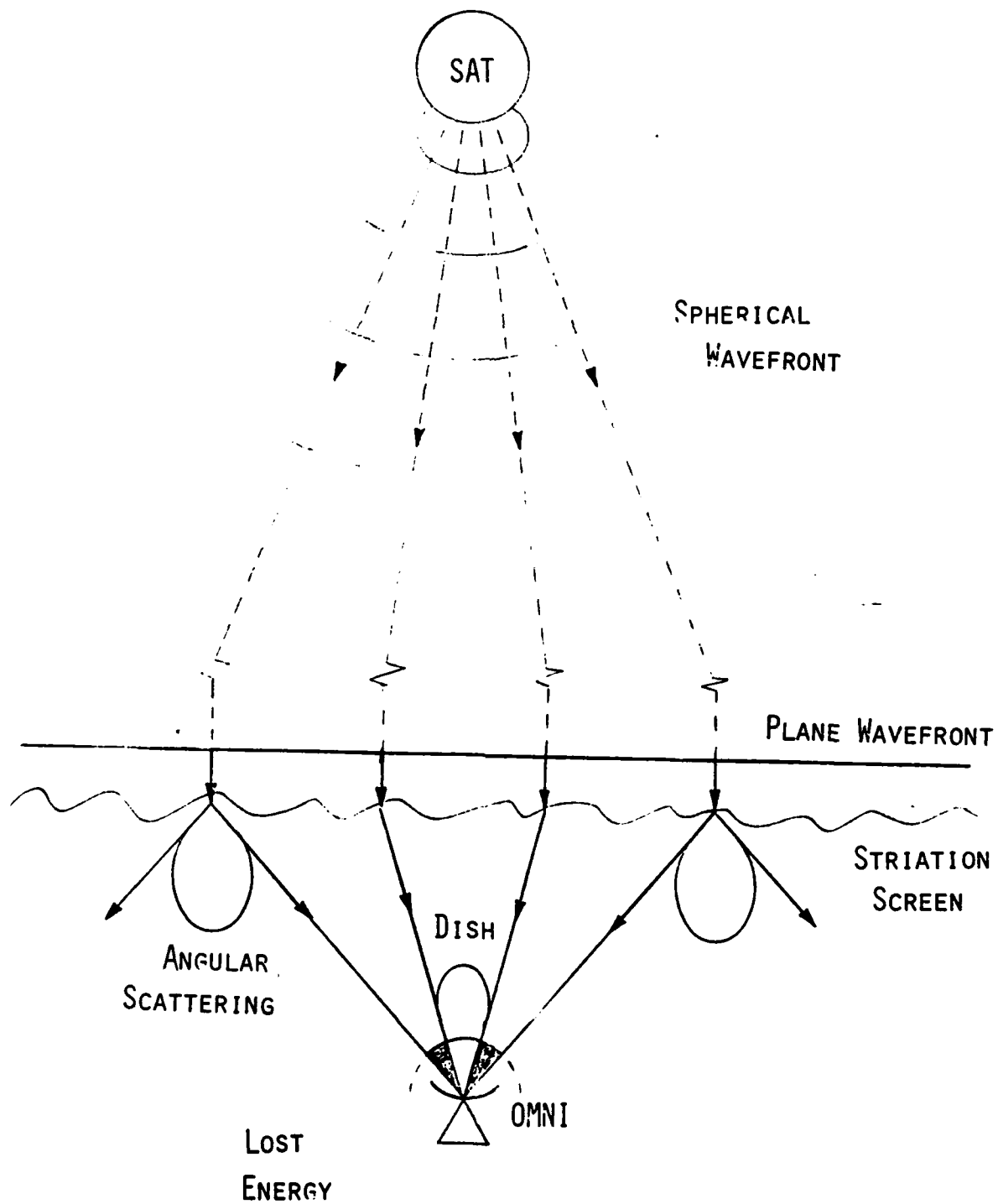
Figure   2.   Downlink Distributed Jamming Effect.

4

algorithms include the Least Mean Square (LMS) gradient based algorithms[4,5], the Howells-Applebaum algorithm[6,7], as well as matrix inversion techniques by direct or recursive methods[2]. Transient performance is also important, but would require much more system specific information to perform an adequate analysis.

Next, the effect of the channel on nulling performance is characterized by subjecting these generic antenna models to jamming signals distorted by sample function representations of simulated two-dimensional (2-D) flat fading. Specific link geometries, transmit/receive antenna beamwidths and carrier frequencies are not addressed. However it is assumed that the channel can be characterized by an equivalent decorrelation distance of the received signal across the receiving antenna's aperture. The Signal-to-Interference plus Noise Ratio (SINR) is used as the measure of performance comparisons. The SINR is first calculated without fading effects, then repeatedly calculated with the effect of many independent fading sample functions. The difference between the nonfading and fading cases is defined to be the performance loss due to fading effects, and the distribution of the loss over many sample functions shows the variance in the loss measurement.

Details of the nulling antenna models are given in Section 2 and the generation of the 2-D fading sample functions is described in Section 3. Plots of the distribution of SINR values resulting from fading effects are presented in Section 4 along with SINR histograms and loss distribution curves which show the percent of time losses greater than X dB can be expected for several degrees of fading severity.

1.3 FUTURE WORK

This "first-cut" analysis shows that the effect of spatial decorrelation across the aperture of nulling antenna can have a significant degrading effect on adaptive nulling antenna performance. This study was limited in scope in several areas which warrant further consideration. These areas are:

1) the effect of different spatial fading sample functions for each jamming source,

2) the transient tracking behavior and resultant noise misadjustment and learning errors for real adaptive systems in time-varying fading,

3) other adaptive nulling algorithms which have gain constraints in desired directions[5],

4) the comparison of adaptive versus non-adaptive weights for the TPAA case,

5) the use of alternative methods in measuring the loss due to phase decorrelation across the aperture including finer sample function sampling of the 2562 point decorrelation function or scaling out the mean amplitude loss before applying the individual sample functions.

SECTION 2

NULLING ANTENNA MODELS

2.1 INTRODUCTION

The two basic adaptive antenna configurations investigated
in this study are the MBA and the thinned phased array antenna.
The MBA configuration is used primarily for continuous area or
spot coverage, whereas the phased array configuration is more
useful for very directive agile-beam type applications.

2.2 MBA MODEL

The receive MBA consists of a waveguide lens of 150
wavelength (λ) diameter, a 16-element square feed horn array in
a 4 x 4 row-column arrangement, and 16 adaptive control loops
(one for each horn). The lens focuses the received wavefront
on the feed elements which are spaced to provide a nominal
0.4-degree singlet (single horn beam) spacing. Figure 3 shows
the nominal rectangular row-column coverage pattern
formed by the 16 horn singlets.
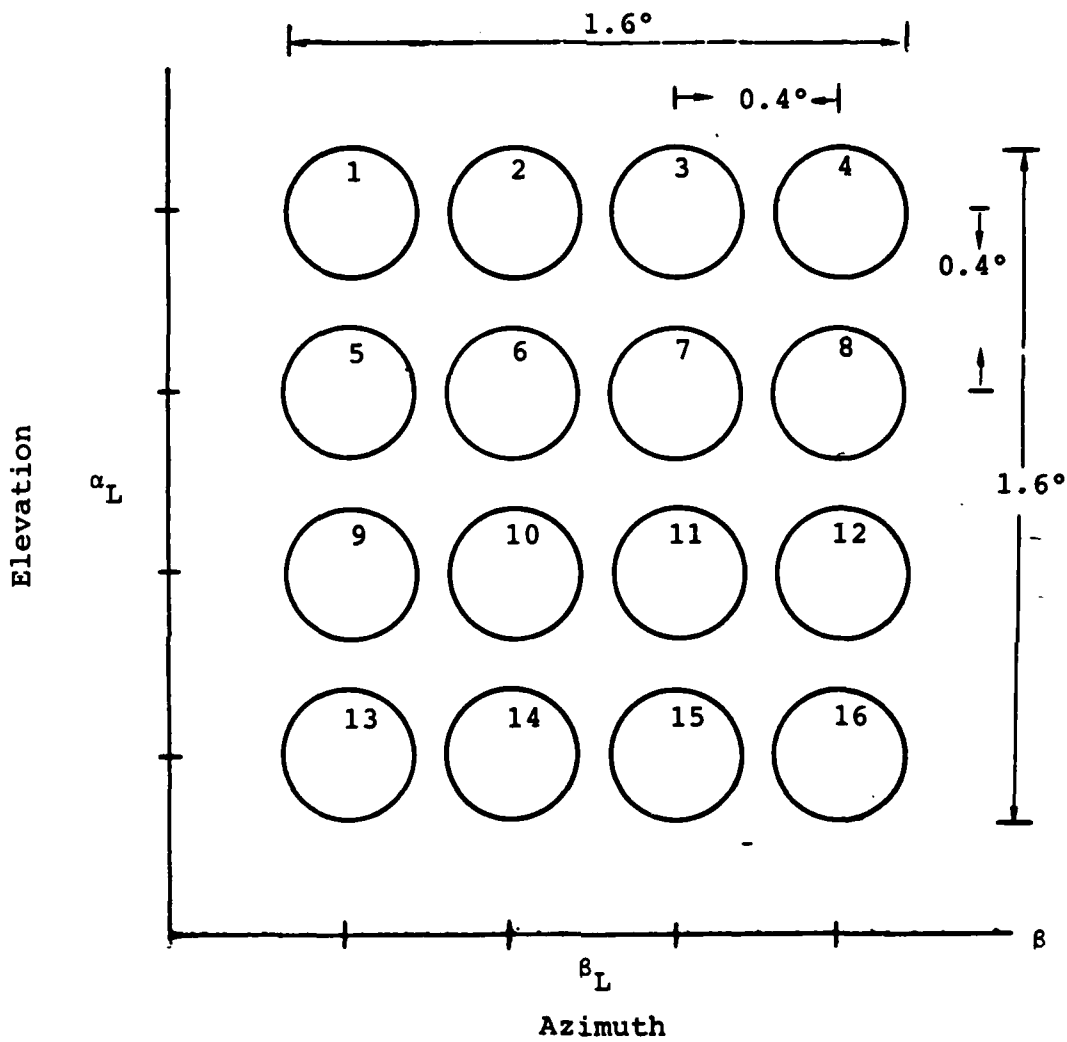
Figure 3.   MBA Coverage Pattern.

The lens aperture feed-horn assembly was modeled as a 2-D planar array of discrete aperture elements at $d = \lambda/2$ spacing. The received beam signal from angular direction (a,b) is calculated as the two dimensional summation of the signal at each discrete lens element location as given by

$$B_{L}(a,b) = \sum_{n=1}^{N} \sum_{m=1}^{N} S(a,b) \exp[j(2\pi/\lambda)\underline{D}_{n,m} \cdot (\underline{e} - \underline{e}_{L})] \quad (2\text{-}1)$$

where

    $S(a,b)$ is the received signal phasor at discrete aperture element (n,m),

    $D_{n,m}$ is the location vector from the aperture center to aperture element (n,m),

    $\underline{e}$ is the unit direction vector from which the signal arrives, and

    $\underline{e}_{L}$ is the unit direction vector toward which the beam is pointed.

The composite antenna pattern is formed by the linear combination of all beams with the appropriate complex weighting factors, W_{L}, and is given by

$$R(a,b) = \sum_{L=1}^{16} W_{L} \cdot B_{L}(a,b) \quad . \quad (2\text{-}2)$$

9

For the nominal steering pattern, all weights are set to (1,0) and the nulling pattern weights are calculated using the adaptive nulling algorithm.

Using the above equations, the composite antenna gain was evaluated and plotted in a three-dimensional perspective plot versus azimuth and elevation angles. Figure 4 shows that the square arrangement of feed horns results in a very regular square shaped gain pattern with a beamwidth of about 1 degree. The gain is relatively constant over an angular square of ±0.5 degrees as appropriate for an area coverage pattern.

2.3 THINNED PHASED ARRAY MODEL

The thinned phased array model used in this study consists of sixteen 6-horn clusters configured as shown in Figure 5. The model consists of 16 clusters arranged in a ring with a diameter of 330 wavelengths. The cluster centers are randomly dithered ±10 λ from equally spaced intervals along the ring. Each of the horns has an earth coverage type pattern and are placed at evenly spaced intervals on a 30 λ diameter circle around the cluster centers. There are only 16 adaptive control weights (one for each cluster) in this model, but all clusters can be simultaneously steered to any desired transmitter location by adjusting nonadaptive weights on the horns of each cluster. Time delay units are then used to coherently synchronize the 16 cluster outputs to obtain the required antenna gain in the direction of the desired signal.

The received beam signal from each cluster can be described by an expression very similar to Equation 2-1 and is given by the sum over all 6 horns comprising a cluster as

10
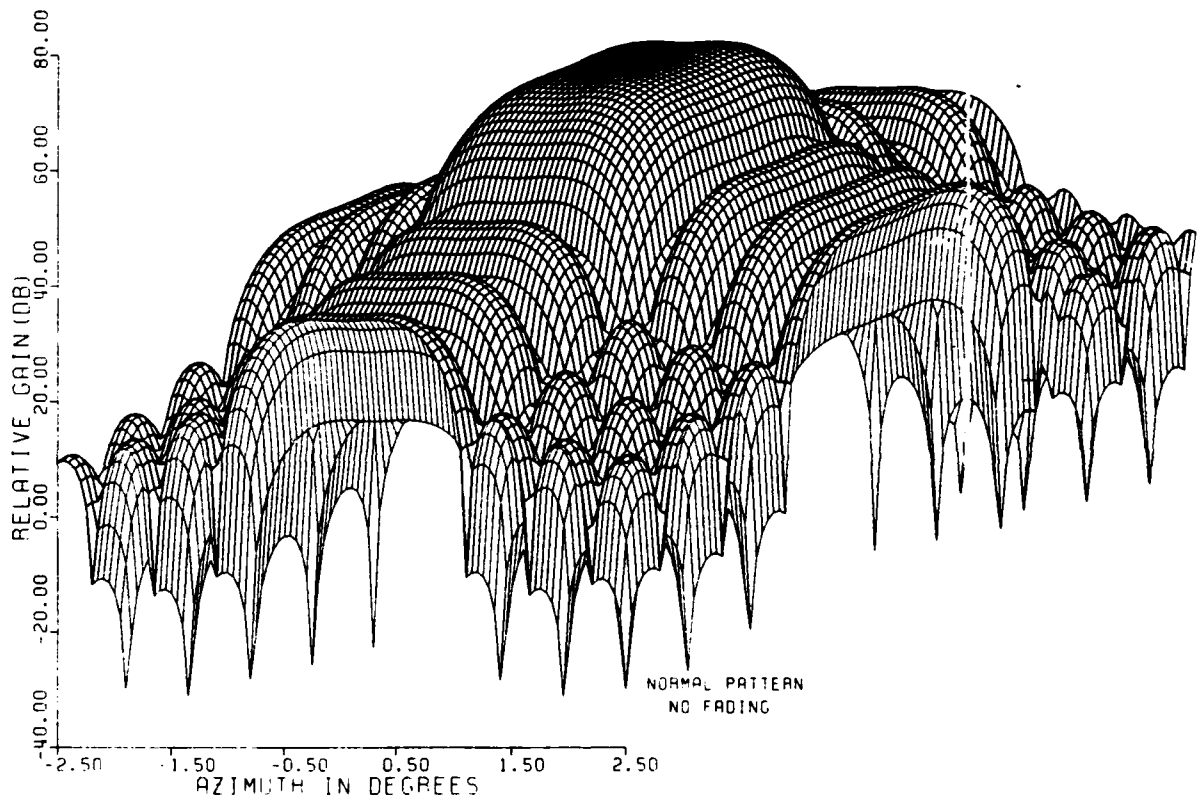
Figure 4.   Composite MBA Pattern.
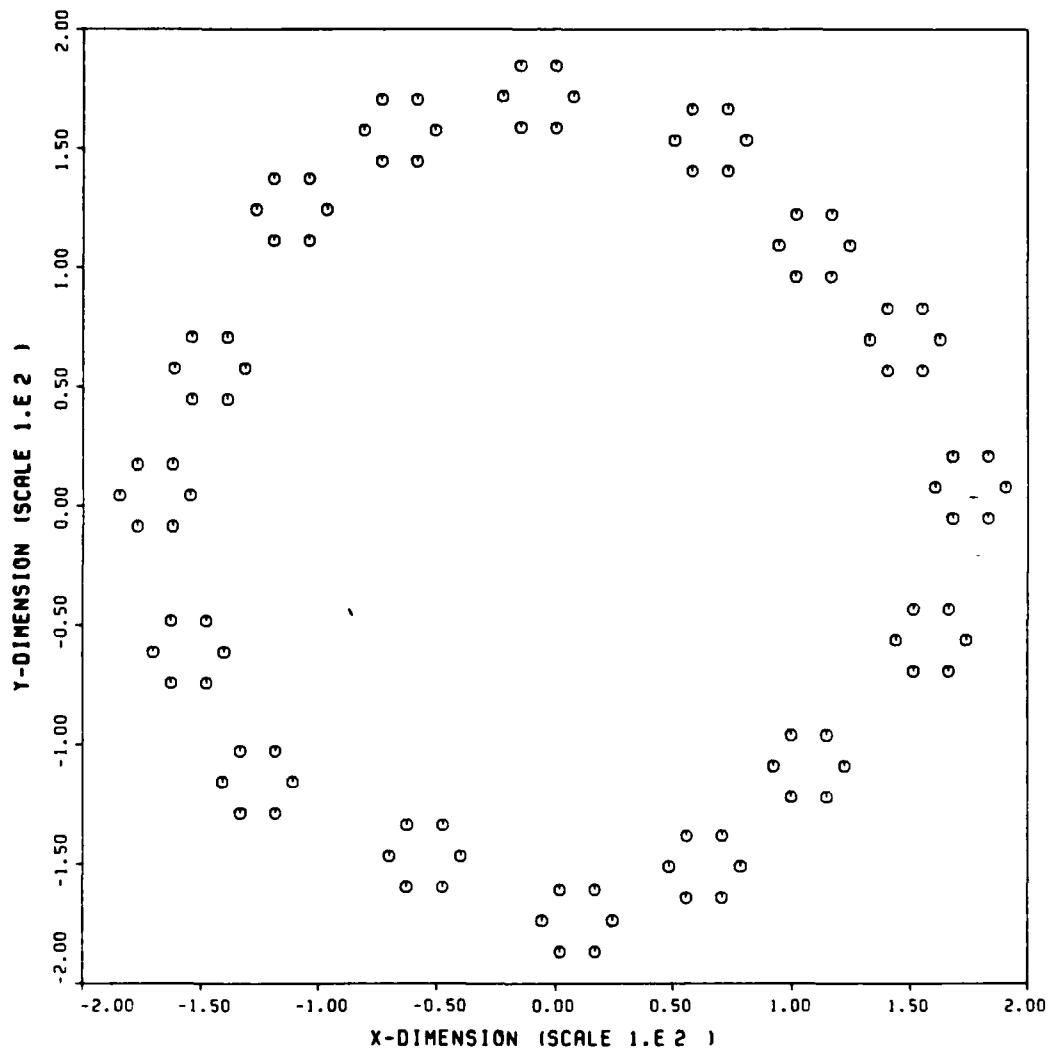
Figure 5. Thinned Phased Array Horn/Cluster Layout.

12

$$B_{L(a,b)} = \sum_{h=1}^{6} H(a,b) \exp[j(2\pi/\lambda)\underline{D}_{h,L} \cdot (\underline{e}-\underline{e}_o)] \qquad (2-3)$$

where

$H(a,b)$ is the received signal for the horn,

$\underline{D}_{h,L}$ is the horn location relative to the antenna center,

$\underline{e}$ is the unit direction vector from which the signal arrives, and

$\underline{e}_o$ is the unit direction vector toward which all the clusters are pointed.

The horn signal is also described by a similar expression and is given by

$$H(a,b) = \sum_{n=1}^{N} S(a,b) \exp[j(2\pi/\lambda) \underline{D}_{n,L} \cdot \underline{e}] \qquad (2-4)$$

where the sum is over N discrete incremental horn aperture subelements separated by $\lambda/2$ spacing, and $\underline{D}_n$ is the horn subelement location relative to the horn center.

The composite antenna pattern for the TPAA like the MBⁱ is formed by the linear combination of all cluster beams with the appropriate complex weighting factors as given by Equation 2-2. Figure 6 shows a 3-D plot of the TPAA gain in dB versus

13
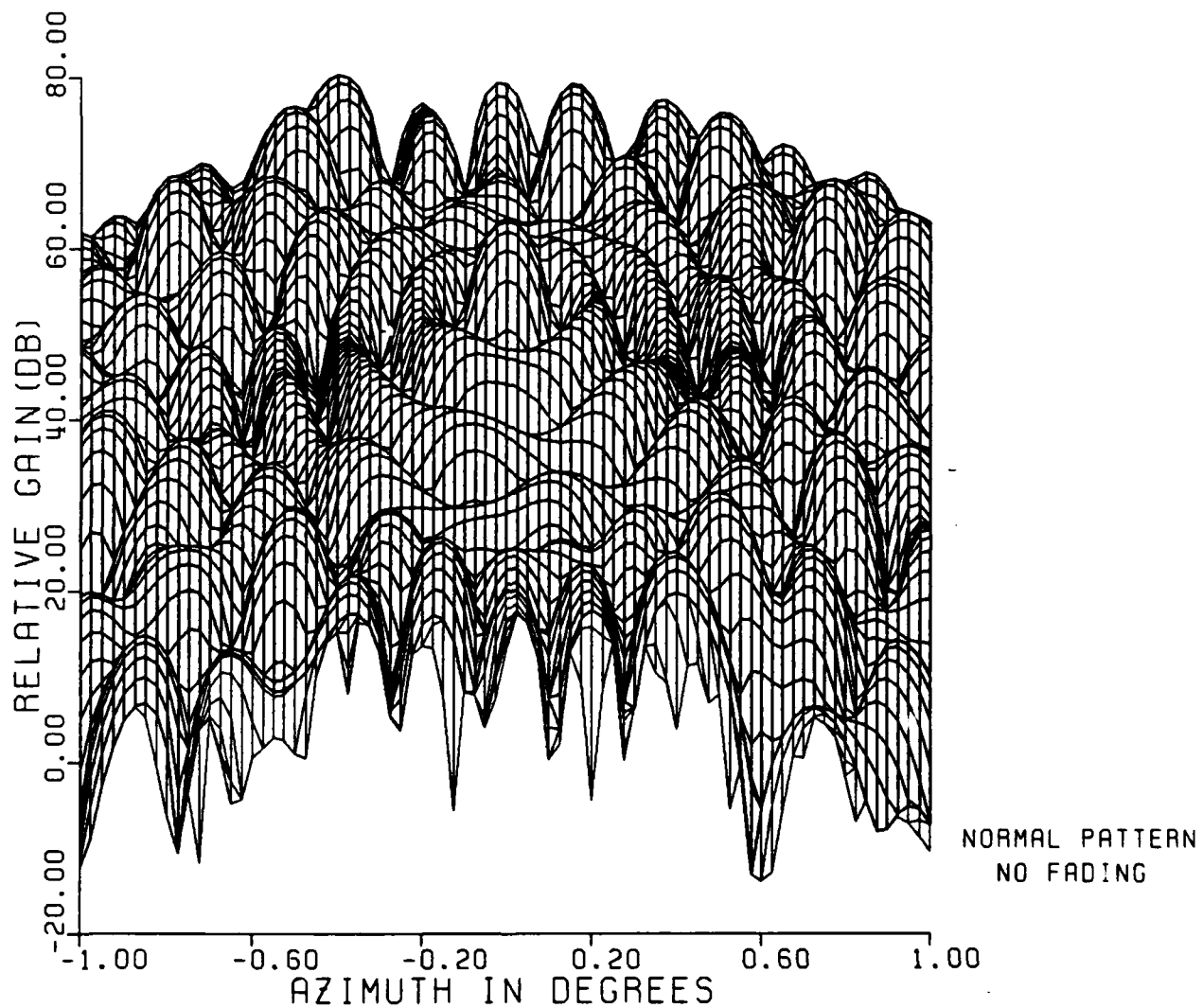
Figure 6.   Composite TPAA Pattern.

14

azimuth and elevation angles. The nominal pattern is shown to
be circular and very directive with beamwidth of only a few
hundredths of a degree pointed at zero degrees azimuth and
elevation. The sidelobe pattern is somewhat irregular caused
by the course spacing between receive aperture clusters.

2.4 NULLING WEIGHT CALCULATION

There are several adaptive interference nulling algorithms
which can be used to compute the weighting factors for use in
Equation 2-2. Remarkably, the steady-state solution toward
which nearly all the adaptive algorithms converge is the
optimum Wiener solution. For the sake of generality and as a
first cut, this study was limited to evaluating steady-state
performance.

The optimal weighting factors used were obtained by direct
matrix inversion of the ideally computed interference/noise
covariance matrix[3]. The complex weight vector is given by

$$\underline{W} = \mu \, \underline{C}^{-1} \underline{S}^{*} \tag{2-5}$$

where

$\underline{C} = E(BB^{T})$ is the interference/noise covariance matrix,

$\underline{S}$ is the nominal beamsteering vector, and

$\mu = 1/(\underline{S}^{T} \underline{C}^{-1} \underline{S}^{*})$ is a normalization factor.

15

The $\underline{B}$ vector used in this study is assumed to be the ideal sum of Equation (2-1) over all possible interference angles-of-arrival plus independent, identically distributed noise on each beam of variance σ_n^2.

The steady-state Wiener solution is not an entirely academic case. It could be representative of a temporally slow fading (relative to the adaptive loop convergence time) case where the adaptive loops are tracking and the solution is near the true Wiener solution. For more rapidly fading cases, the Wiener solution also serves as the limiting case on performance. While the algorithm tries to converge toward the current optimal solution, the optimal solution is changing with time so that it never fully converges to the optimal (sometimes called learning error). Another error called misadjustment error results from noise in the adaptive control loop equations.

2.5 POST NULLING ANTENNA PATTERN PLOTS

The composite antenna gain values were computed using the nulling weights computed by the above equations for both MBA and TPAA configurations with two jammers located at zero degrees elevation and 0.15 and 0.60 degrees azimuth.

The TPAA gain values in dB, plotted in a 3-D representation shown in Figure 7, show two deep nulls formed in the jammer directions while the rest of the gain pattern remained relatively unchanged. Figure 8 plots the change in gain from the nominal pattern to the nulled pattern in 3-D to more clearly show the sharpness of the nulling beams formed by the inverse covariance matrix transformation of the nominal

16
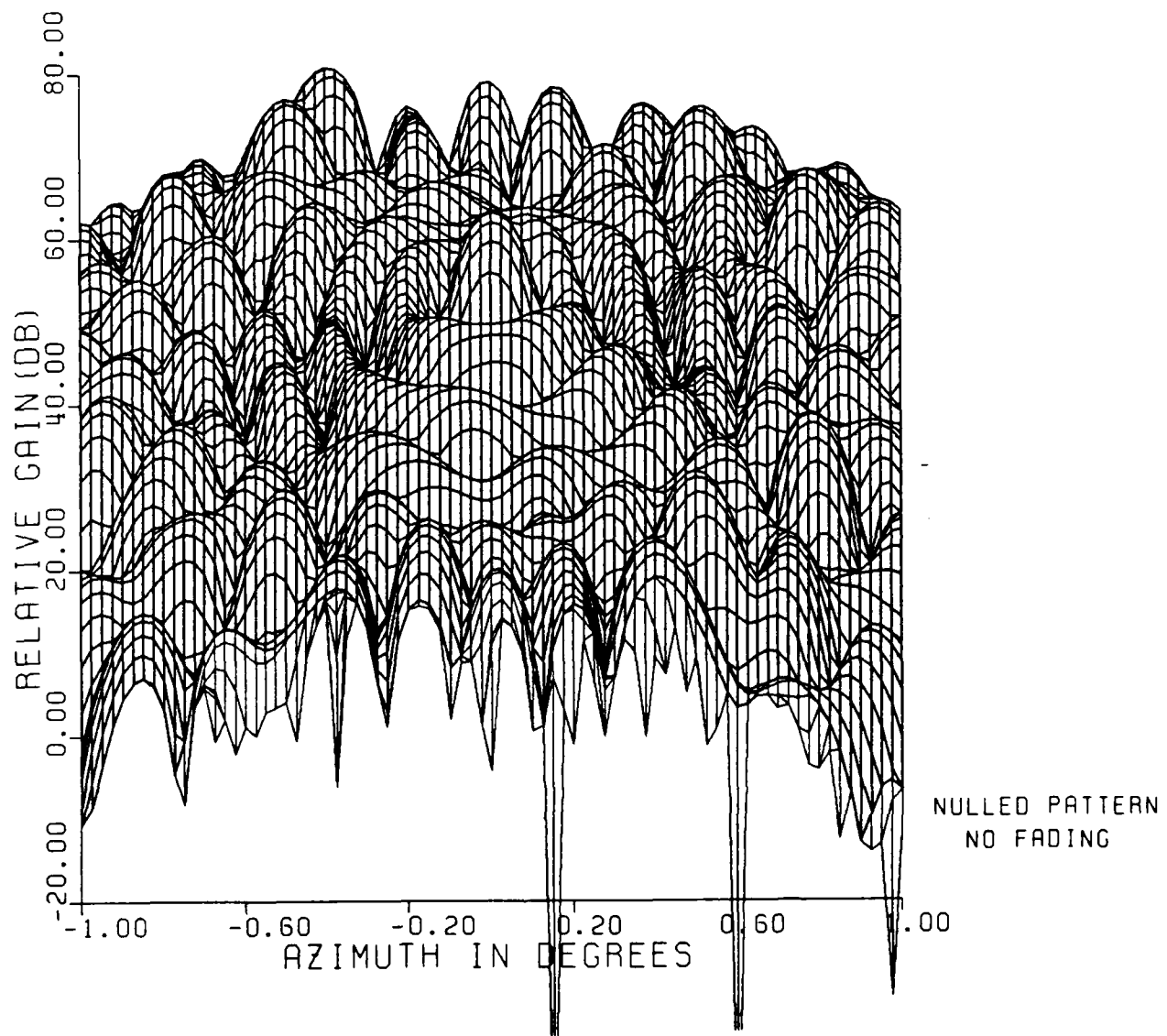
Figure 7.   Nulled TPAA Gain Pattern.

17

Figure   8.   TPAA Pre/Post Gain Change Pattern.

18
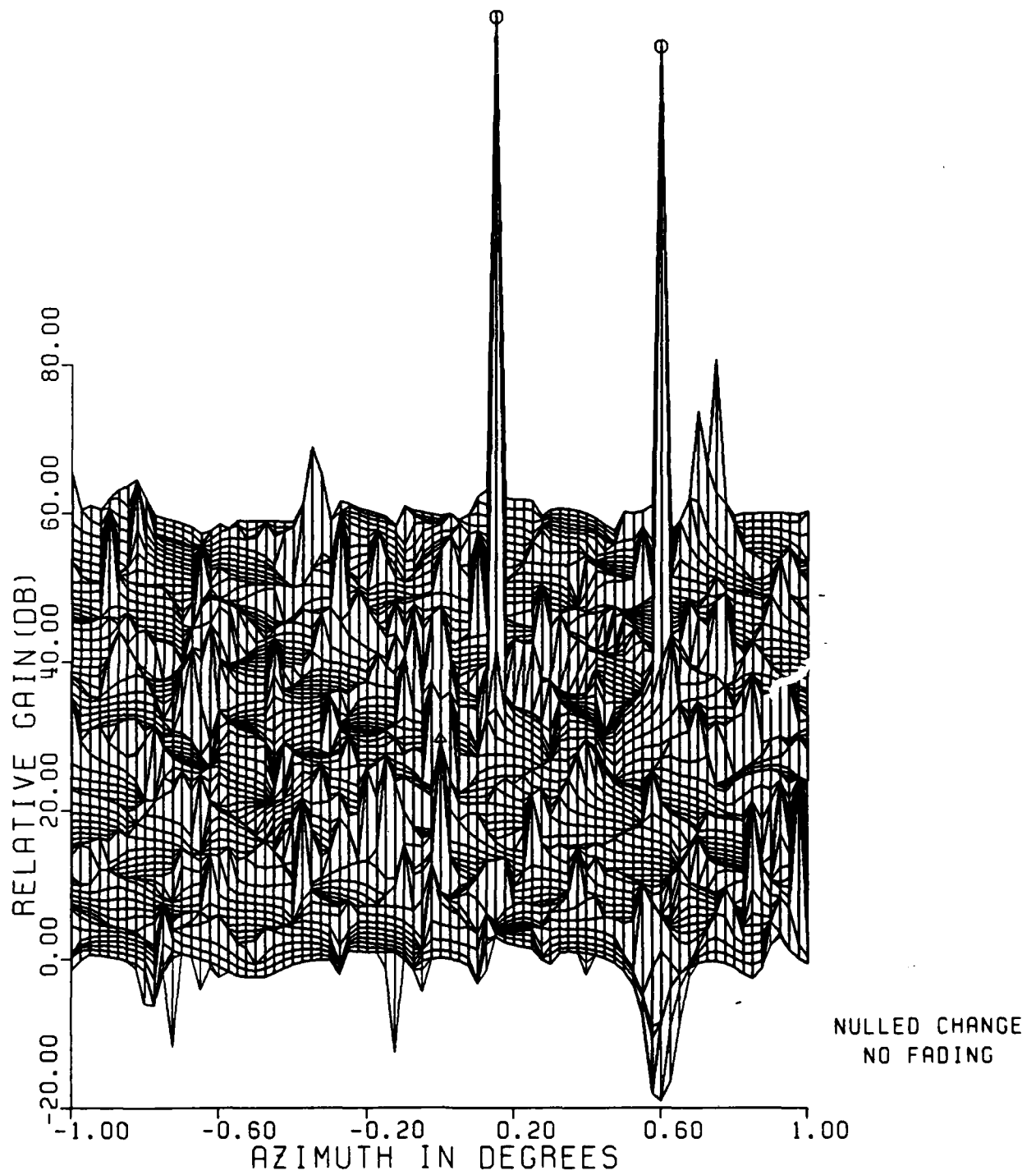
steering vector. The triangle symbol marks the user angular
direction and the two octagons mark the jammer angular
directions.

Figures 9 and 10 are the equivalent nulled and gain change
pattern plots for the MBA configuration. Note that these nulls
appear to be somewhat wider than those of the TPAA and sidelobe
gain variations were more pronounced.

RELATIVE GAIN (DB)

AZIMUTH IN DEGREES

NULLED PATTERN
NO FADING
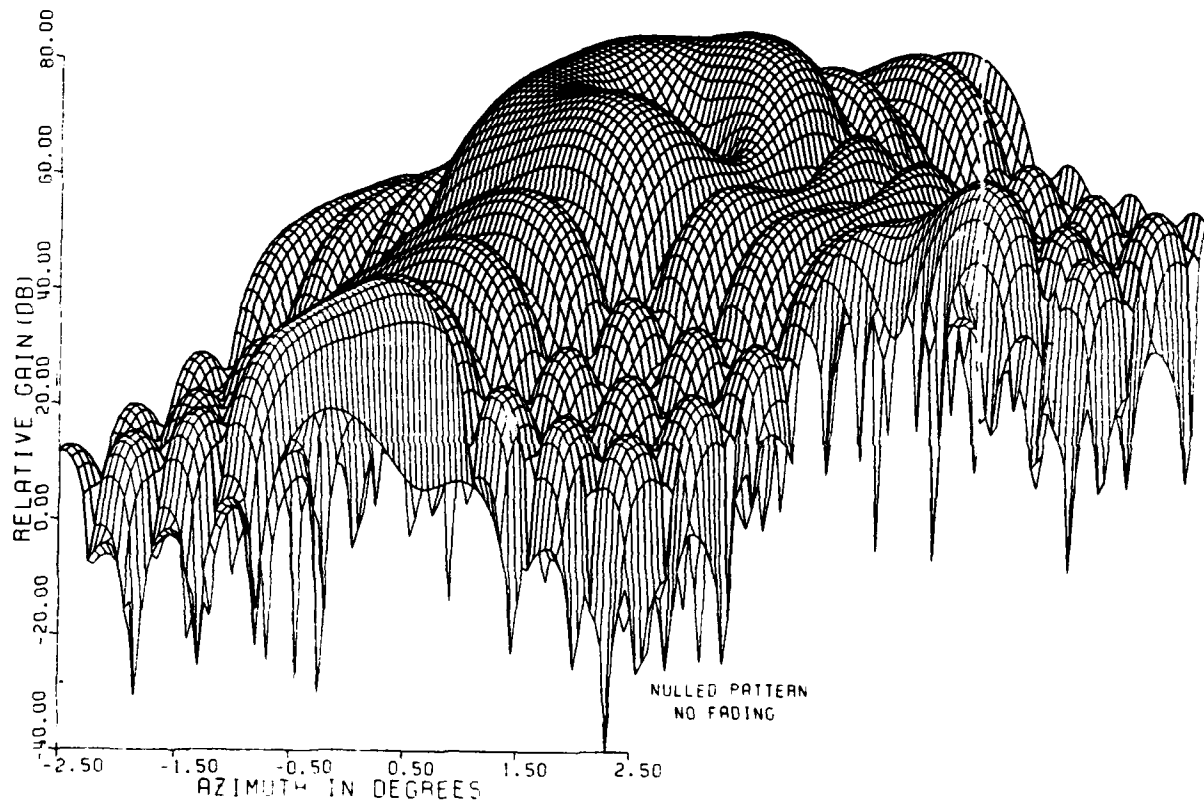
Figure 9. Nulled MBA Gain Pattern.

20
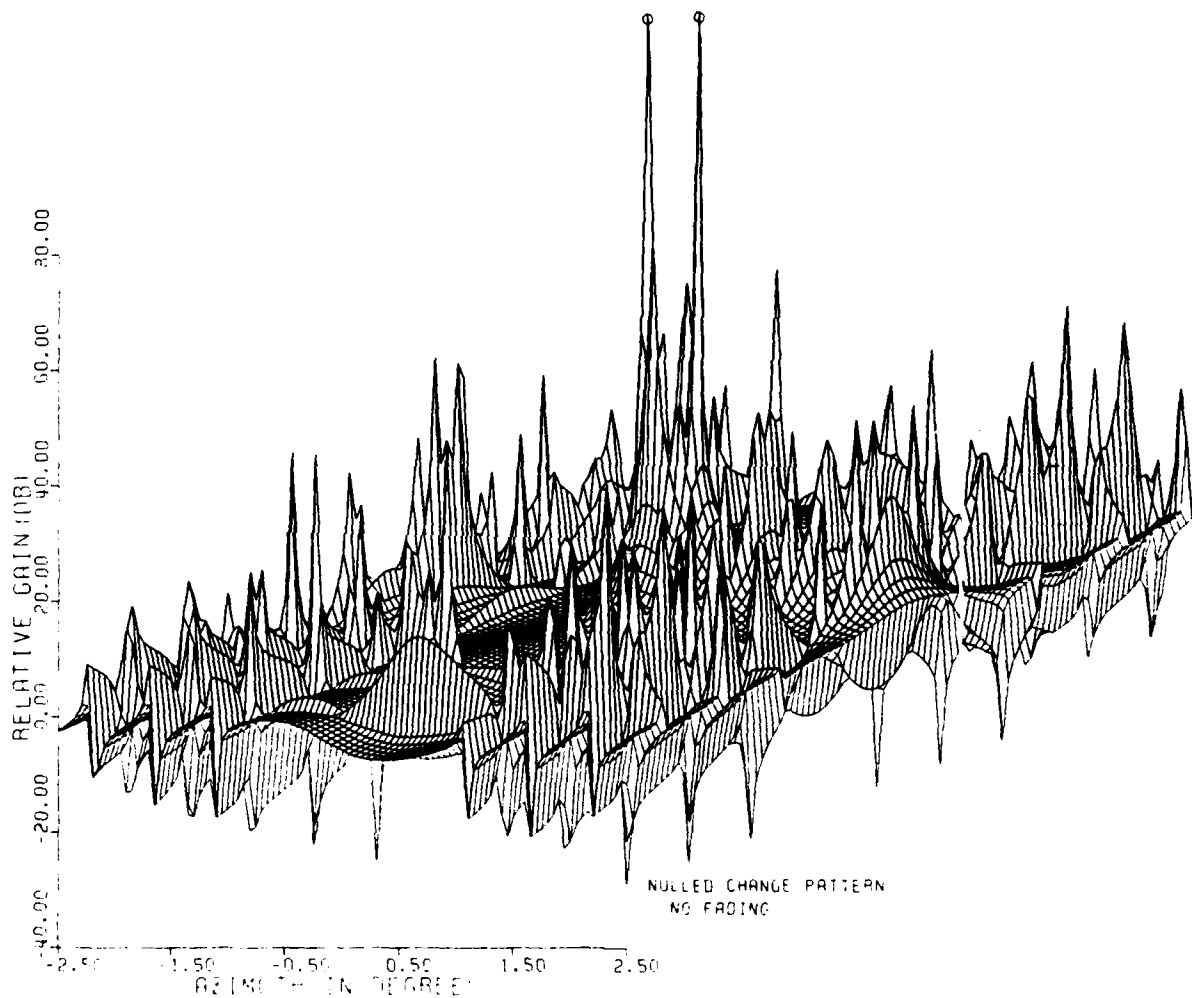
Figure 10.   MBA Pre/Post Gain Change Pattern.

SECTION 3

TWO DIMENSIONAL, TWO-POLE SPATIAL DECORRELATION MODEL

3.1 MODELING

The fading process is actually a spatial phenomenon whose temporal characteristics principally arise from the relative velocity of the medium with respect to the signal propagation path. The emphasis of this study was to ascertain the effect of spatial decorrelation rather than temporal decorrelation effects on nulling performance. Thus, 2-D isotropic spatial fading random processes were used to model the channel in this study. The spatial fading sample functions had autocorrelation function given by

$$R(r) = (1 + K|r|/l_o) \exp(-K|r|/l_o) \qquad (3-1)$$

where l_o is the decorrelation distance of the fading random process at the nulling antenna aperture, r is the 2-D radial offset parameter, and $K = 2.146$.

A large 2-D array containing many independent 2-D fading random process sample functions were generated for this study using Fourier transform techniques. These sample functions were then used to distort received jammer phase and amplitude across the face of the nulling antenna's aperture. It is believed that the evaluation of performance for many independent sample functions will provide more accurate

22

information about the statistical distribution of the spatial
decorrelation effects than a simpler power distribution
averaging approach would provide.

The effect of the channel on the antenna array elements
was assumed to be identical for all jammers. A complex phasor
at the location of each array element is computed via
interpolation of the 2-D sample function and this phasor
multiplicatively corrupts the composite received signal at each
antenna element. The modified beam vector is then used to
calculate the distorted covariance matrix which is in turn used
to compute the channel distorted nulling weights.

SECTION 4

SINR PERFORMANCE WITH SPATIALLY DECORRELATED
CHANNEL SAMPLE FUNCTIONS

4.1 SINR PERFORMANCE MEASURE

The Signal-to-Interference plus Noise Ratio (SINR) is a convenient measure of a nulling antenna's ability to suppress undesired interfering signals with respect to a desired signal of interest in a nonfading environment. A simpler null depth calculation is not as useful in evaluating communication system performance because jammer suppression, the relative noise floor level, and gain in the direction of the desired signal collectively affect the system performance.

The SINR is defined as

$$\text{SINR} = \frac{P_s}{P_{I\&N}} = \frac{P_s}{\underline{W}^T \underline{C} \underline{W}^*} = P_s \underline{S}^T \underline{C}^{-1} \underline{S}^* \qquad (4\text{-}1)$$

where

P_s is the received signal power,

$P_{I\&N}$ is the interference + noise power after adaptation,

$\underline{C}$ is the interference/noise covariance matrix, and

$\underline{S}$ and $\underline{W}$ are the nominal steering and nulling weight vectors, respectively.

24

The equation is the same for jammer nulling in fading channels
except that the distorted channel covariance matrix and weight
vector are used in the fading disturbed SINR calculation.

4.2 SINR DEGRADATION IN FADING CHANNELS

The measurement of the antenna's nulling capability in
fading is complicated by the fact that in addition to the
spatial decorrelation distortion of the received jamming
signal, all the jamming signals and the desired signal levels
may also fluctuate. Thus, changes in SINR are simultaneously
caused by several effects and the incremental contribution of
each effect is difficult to ascertain.

In this study, it was assumed that the jammers and
sometimes the desired signal transmitter are in relatively
close proximity of each other so that the same fading effects
are applied to all. Independent fading for each signal source
is a possibility but it is not addressed here.

The severity of the channel decorrelation distortion is
characterized by a normalized stress parameter given by

$$S = D/l_o \qquad\qquad (4-2)$$

which is the ratio of the antenna aperture outer diameter (D)
to the channel decorrelation length, l_o. It can also be viewed
as the number of channel decorrelation lengths across the
aperture and larger S values represent more severe distortion.

For sufficiently small channel stress values (S<<1), the loss due to spatial decorrelation distortion across the receiving antenna aperture is expected to be negligible, and the resulting loss distribution curve for this case characterizes the SINR loss due solely to fluctuations in signal level. As the channel stress parameter value increases, the aperture decorrelation distortion increases and its effect becomes more noticeable. The dB difference between the loss at different stress values represents the additional loss strictly due to the spatial decorrelation distortion.

4.3 SINR SAMPLE FUNCTION HISTOGRAMS AND LOSS CURVES

A two-dimensional spatially decorrelated sample function was generated in a 256 by 256 complex array with 10 samples per decorrelation length, l_o. The effect of many nearly independent channel subsample functions were extracted from this larger set by using independent subsections. The channel subsections used were separated by about one decorrelation length in a 25 x 25 grid pattern over the 256^2-element array.

The SINR which resulted from each of the channel sample functions were tabulated and a histogram of the SINR value spread was plotted. Assuming that the distribution of SINR events is fairly representative of the true density, a loss distribution curve showing percent outage for SINR losses of X-db or more with respect to nonfading SINR was computed and plotted for several channel stress values.

4.3.1 TPAA Configuration - Jammers and Signal Fading

Figures 11 and 12 show the histogram of SINR values for the TPAA configuration with signal and jammers all identically fading with channel stress values of 0.005 and 0.8, respectively. The jamming scenario consisted of twelve 20 dB jammers located at zero degrees elevation and 0.150, 0.225, 0.325, 0.425, 0.525, 0.600, 0.700, 1.050, 1.250, 1.375, 1.550, and 1.750 degrees azimuth. The noise floor variance was set at -7 dB. These histograms show that the fading causes a dispersion in the SINR from its nonfading nominal value of 7.21 dB. The SINR histogram exhibits a tendency to improve SINR as well as degrade SINR although the latter predominate causing the histogram to skew to the left. The higher stress case shows more dispersion than the lower stress case.

Figure 13 shows the loss distribution curves for the TPAA configuration for stress values ranging from 0.005 to 0.8. The SINR loss at S=0.005 is shown to be significant, however, most of this loss is caused by signal amplitude fluctuations relative to the fixed noise floor. The nulling capability of the antenna has not been degraded since there is essentially no spatial decorrelation distortion at this stress level.

The loss due to spatial decorrelation distortion is only evident for larger stress values. It is measured as the increased SINR loss over and above the loss shown for S=0.005. This loss appears to be substantial for a significant percent of the time. The SINR loss values for spatial decorrelation distortion stress levels of 0.2, 0.4, and 0.8 and are tabulated in Table 4.3-1. The term percent exceedance refers to the percent of time the loss exceeds the value shown. For example,
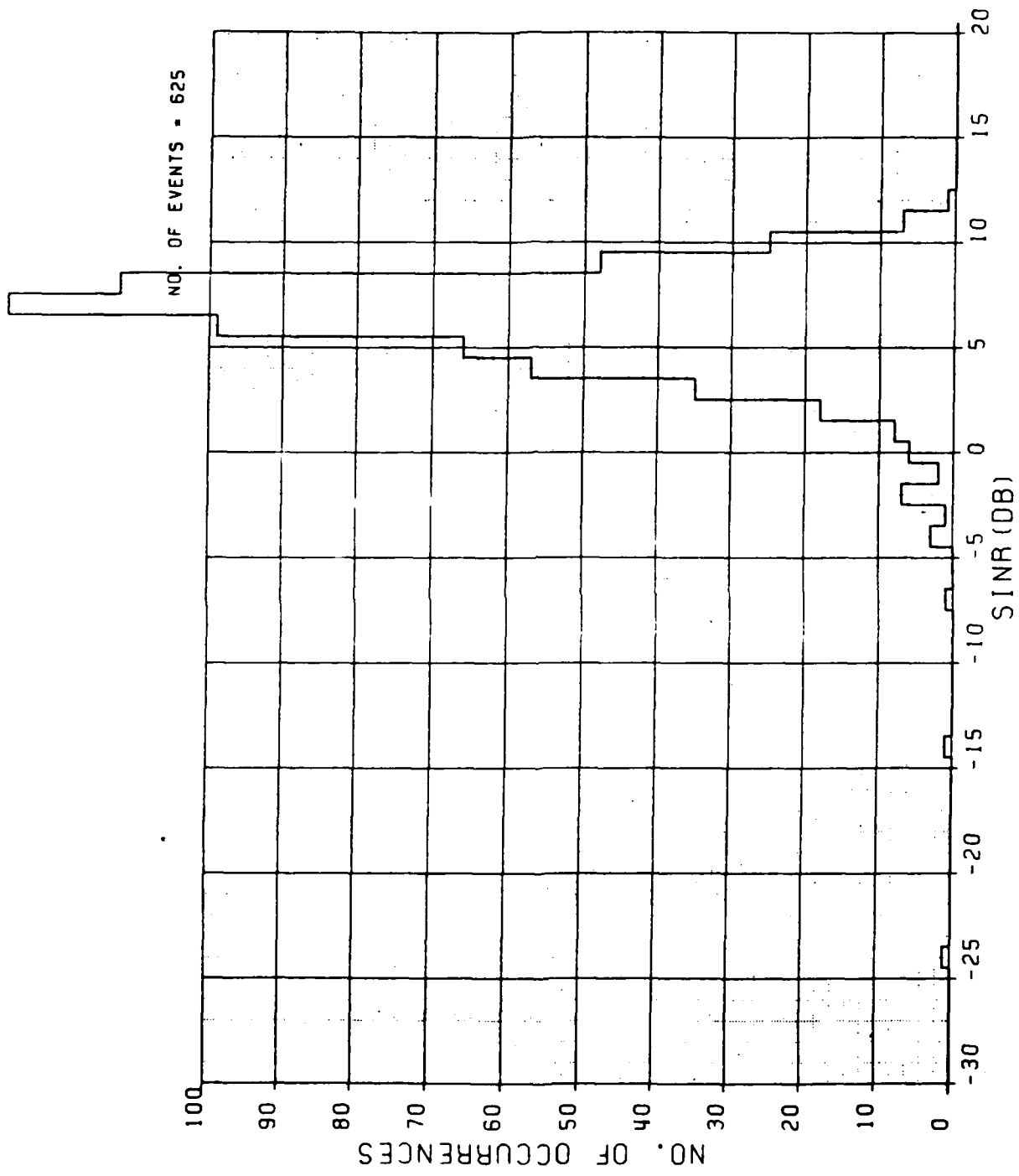
Figure 11. TPAA Configuration Histogram, Signal and Jammers Fading, S=0.005.

28
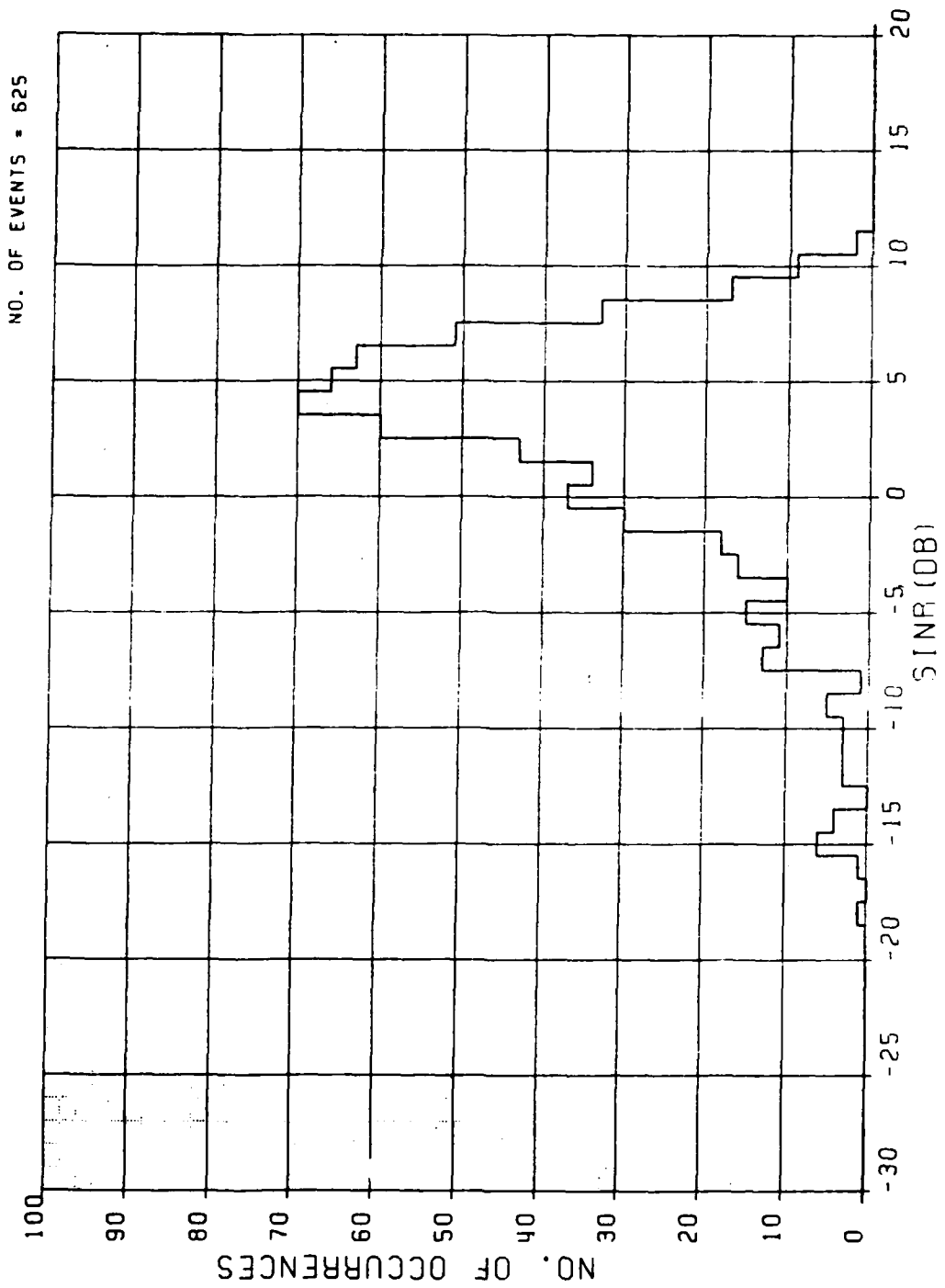
Figure 12.   TPAA Configuration Histogram, Signal and Jammers Fading, S=0.8.

29
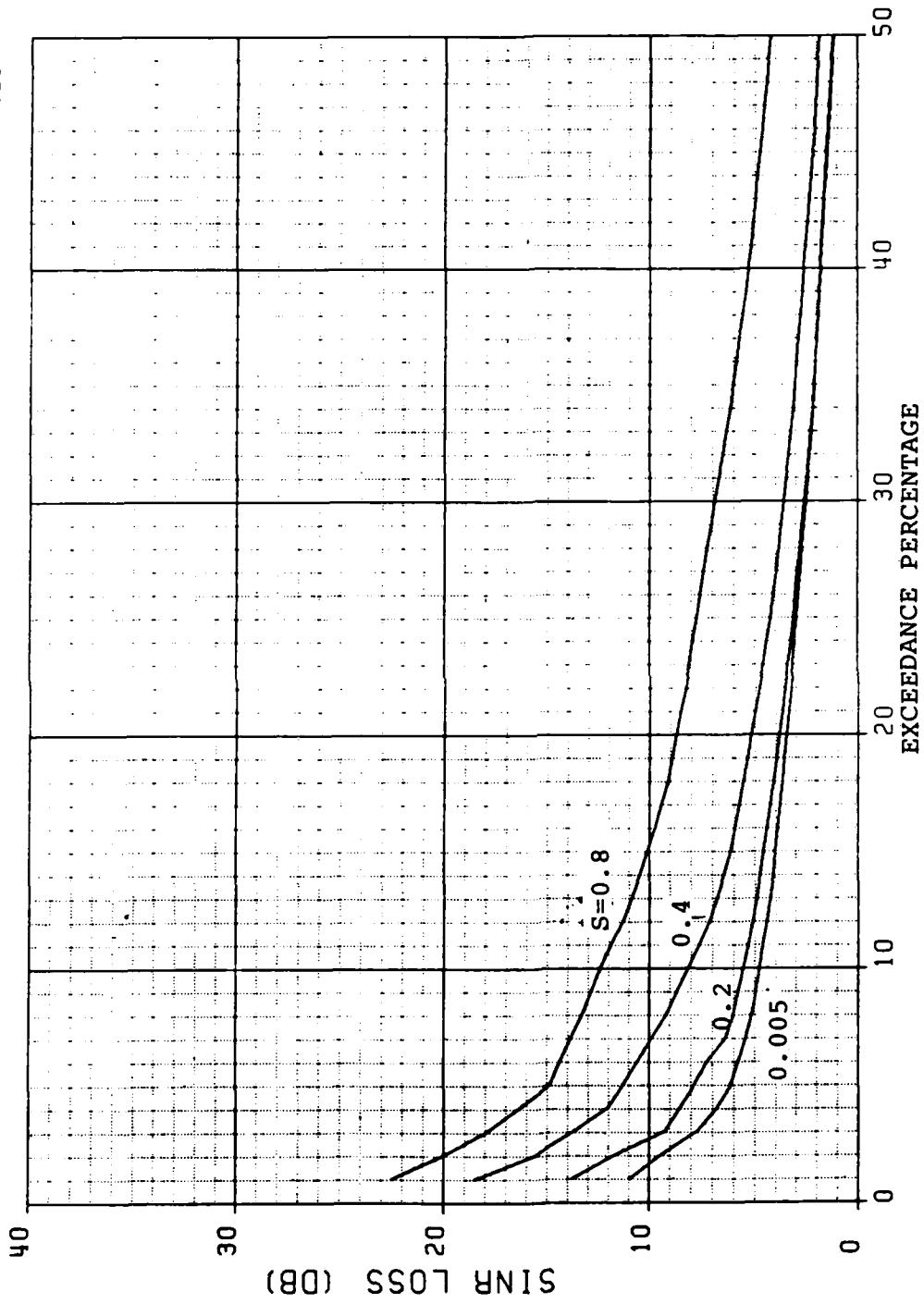
Figure 13.   TPAA Configuration Loss Distribution, Signal and Jammers Fading.

for a stress level of 0.8, the SINR is degraded by 12.5 dB or more 10 percent of the time.

The sensitivity of this loss to the channel stress parameter value is inversely related to the relative noise floor variance. That is, SINR distortion loss is larger when the difference between the noise floor variance and the jammer power levels is greater. This observation is reminiscent of how the bit error rate sensitivity to fade rate is related to the nominal bit energy-to-noise density ratio.

Table 4.3-1 Spatial Decorrelation SINR Loss in dB
TPAA Configuration (Increase in SINR
loss over loss for S=0.005)

$$S = D/l_o$$

	0.2	0.4	0.8
1%	3	7	11
5%	2	5	9
10%	1	3	7
20%	0.5	1.5	5

Percentage Exceedance

4.3.2 TPAA Configuration - Jammer Fading, Signal Not Fading

As an alternative fading scenario, the case where only the jamming signals are affected by the fading while the desired signal is not fading was considered. Figures 14 and 15 show the histograms of SINR values for channel stress values of 0.005 and 0.8, respectively. Since the desired signal is not fading, much of the large SINR loss events which caused the low SINR tails in Figures 11 and 12 no longer occur. The jammers fading only histograms still show a dispersion in SINR, but the spread tends to toward an SINR gain instead of a loss. Again this occurrence is a result of the temporal amplitude level fluctuations due to fading jammers rather than the effect of phase decorrelation across the aperture.

Figure 16 shows the corresponding loss distribution curves for the TPAA configuration for stress levels ranging from 0.005 to 0.8. The curves show virtually no decorrelation distortion loss for values of stress ranging from 0.005 to 0.4 and a gain of about 1 dB for a stress value of 0.8 which is not understood at this time. It may be that the steady state nulling solution can provide a better SINR due to the requirement for a broader, less deep, null for the angularly spread jammers. A truely adaptive antenna may or may not be able to converge to this value.

4.3.3 MBA Configuration - Jammers and Signal Fading

Figures 17 and 18 show the histograms of SINR values for the MBA configuration with signal and jammers all identically fading with channel stress values of 0.005 and 0.8,

32
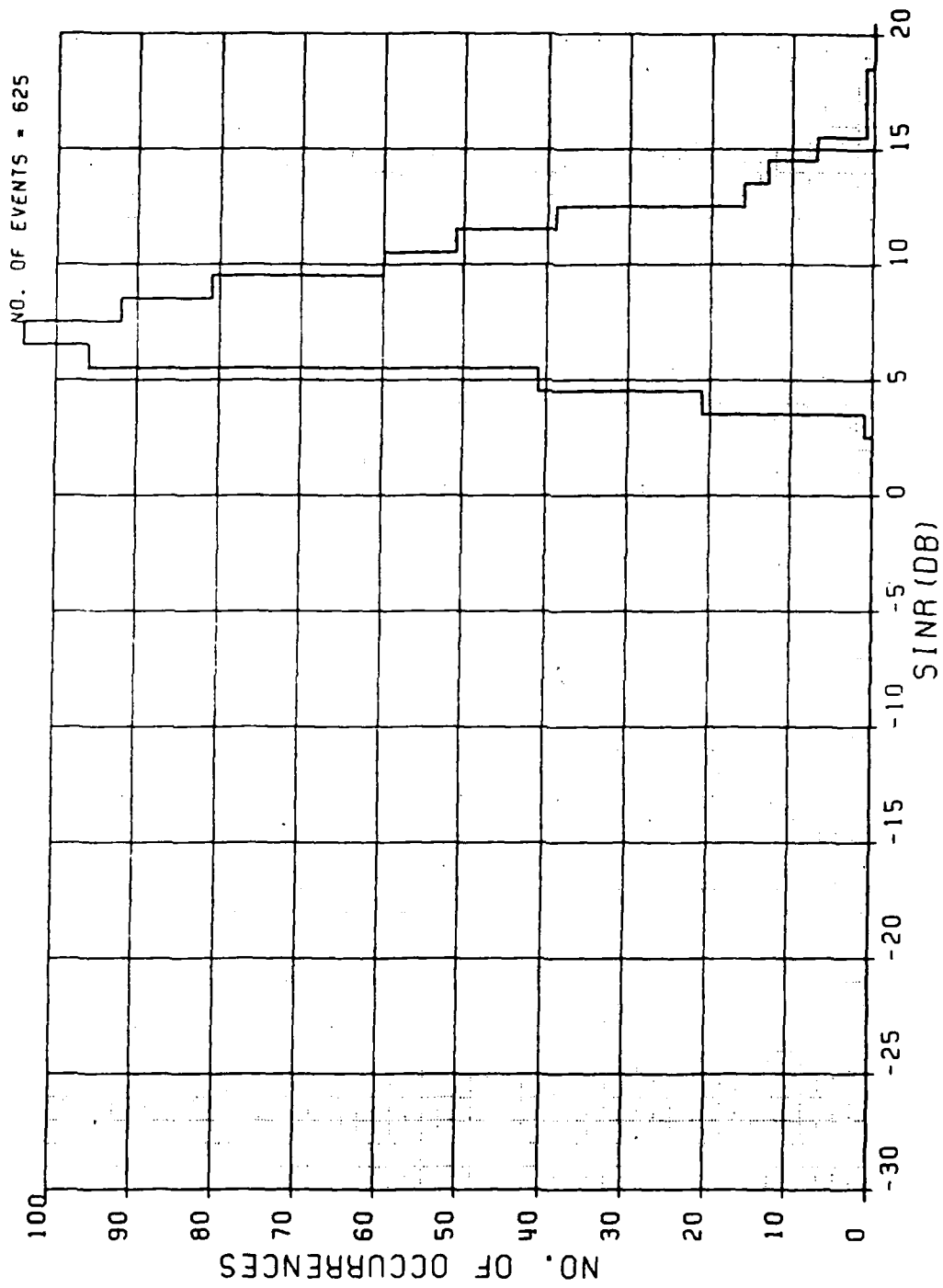
Figure 14. TPAA Configuration Histogram, Jammers Fading, Signal Not Fading, S=0.005.

33
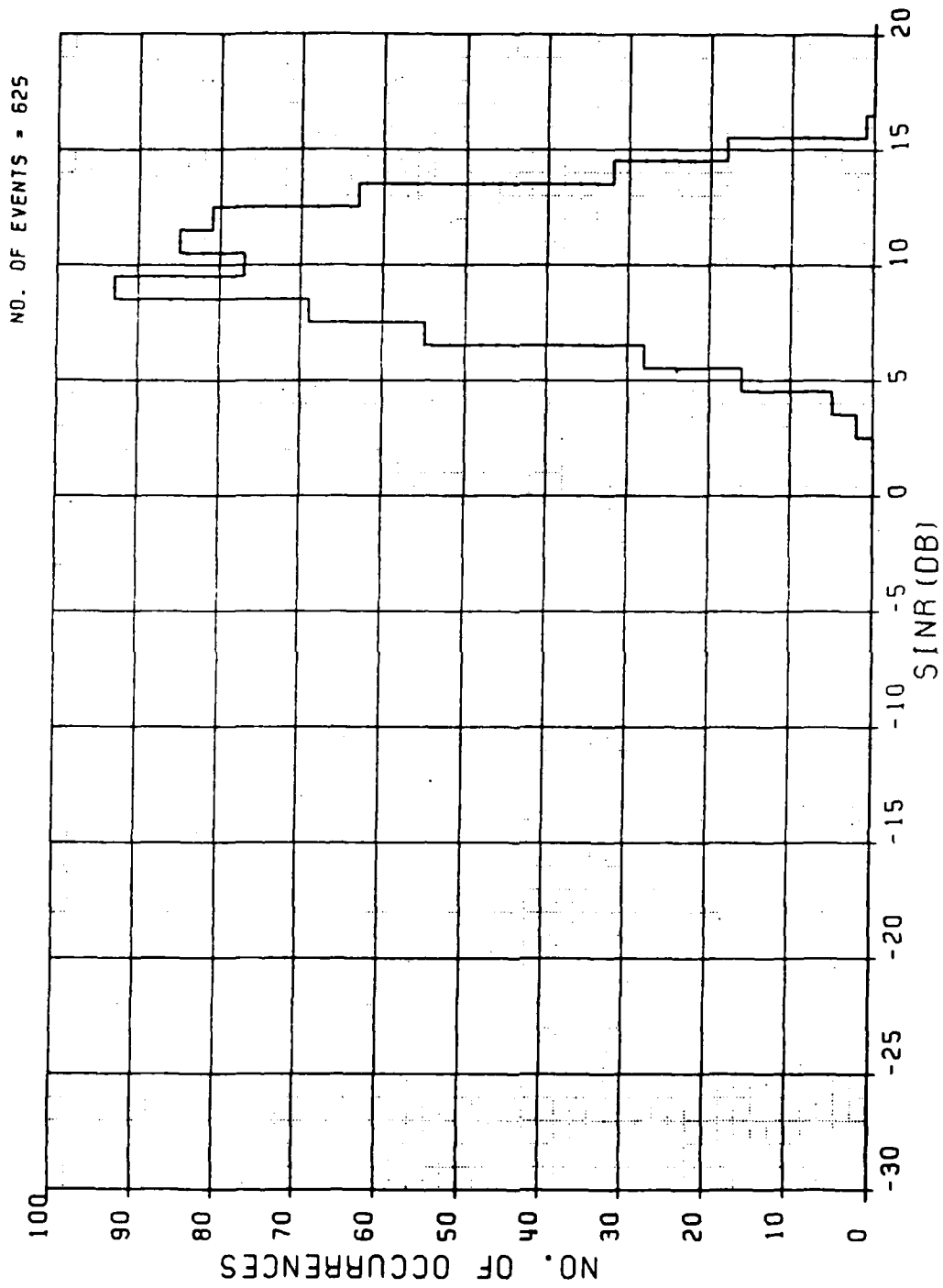
Figure 15.   TPAA Configuration Histogram, Jammers Fading, Signal Not Fading, S=0.8 .

34

REF. SINR(DB) = 7.21

SINR LOSS (DB)

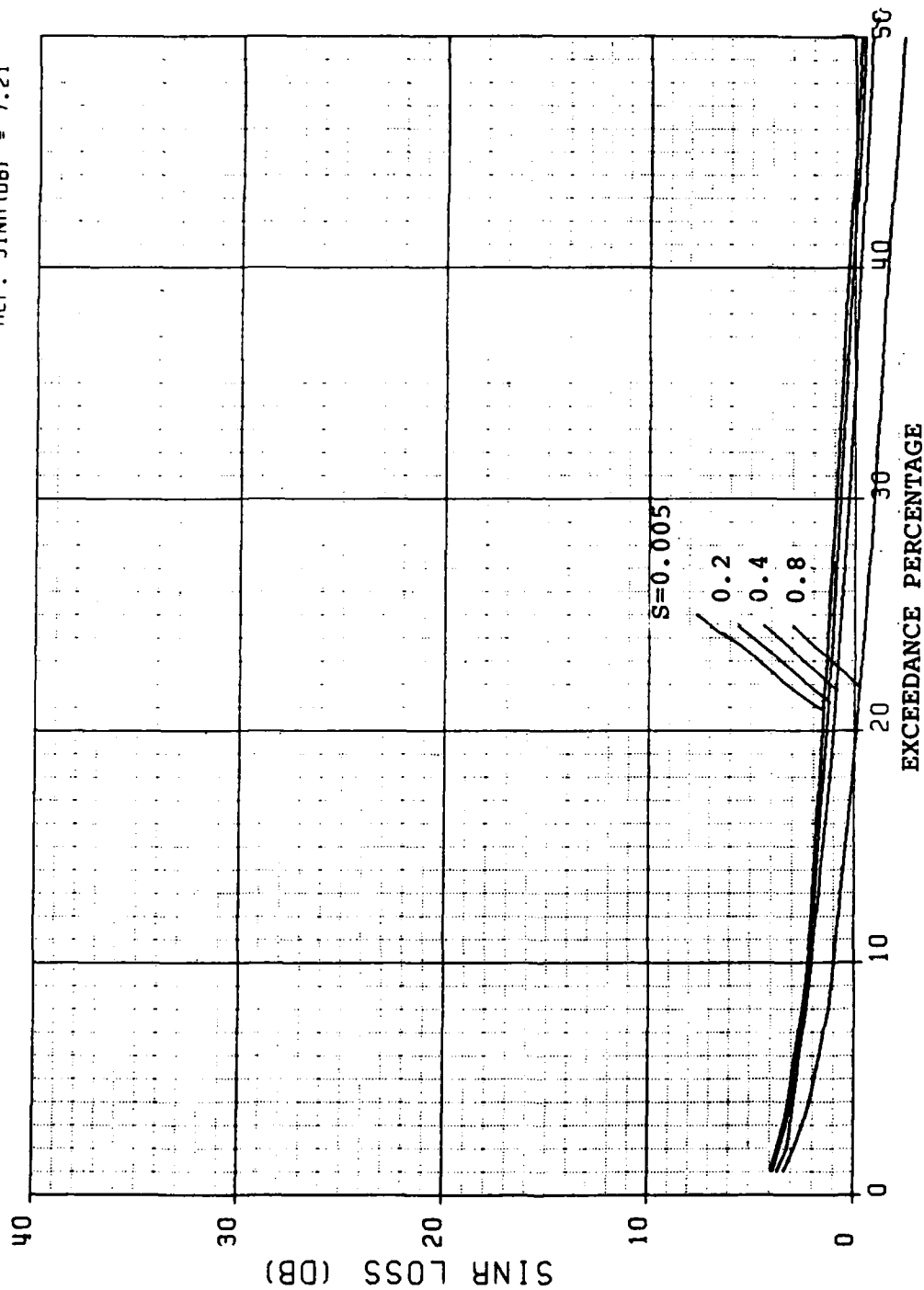EXCEEDANCE PERCENTAGE

S=0.005
0.2
0.4
0.8

Figure 16.   TPAA Configuration Loss Distribution, Jammers Fading, Signal Not Fading.
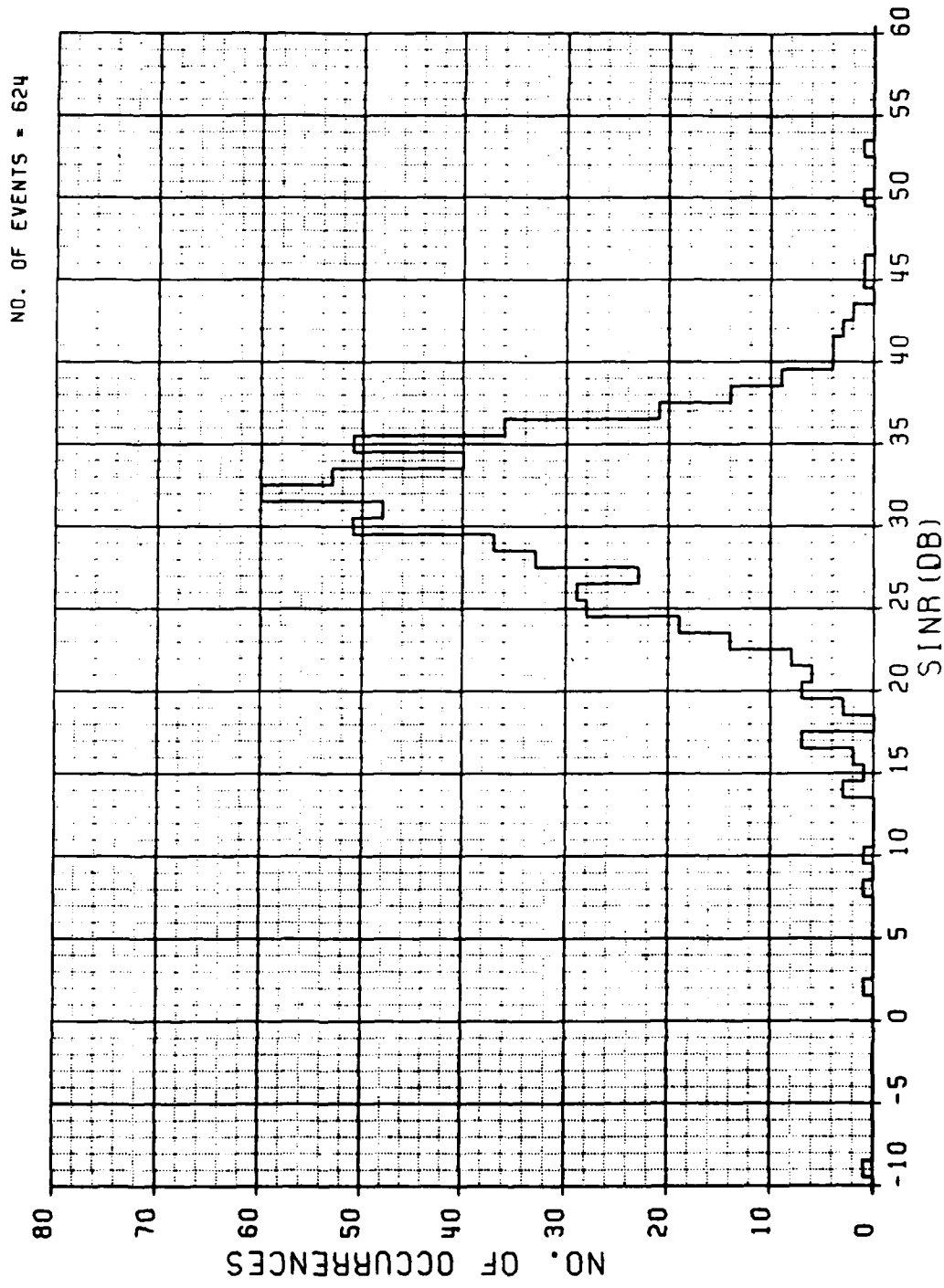
Figure 17. MBA Configuration Histogram, Signal and Jammers Fading, S=0.005.

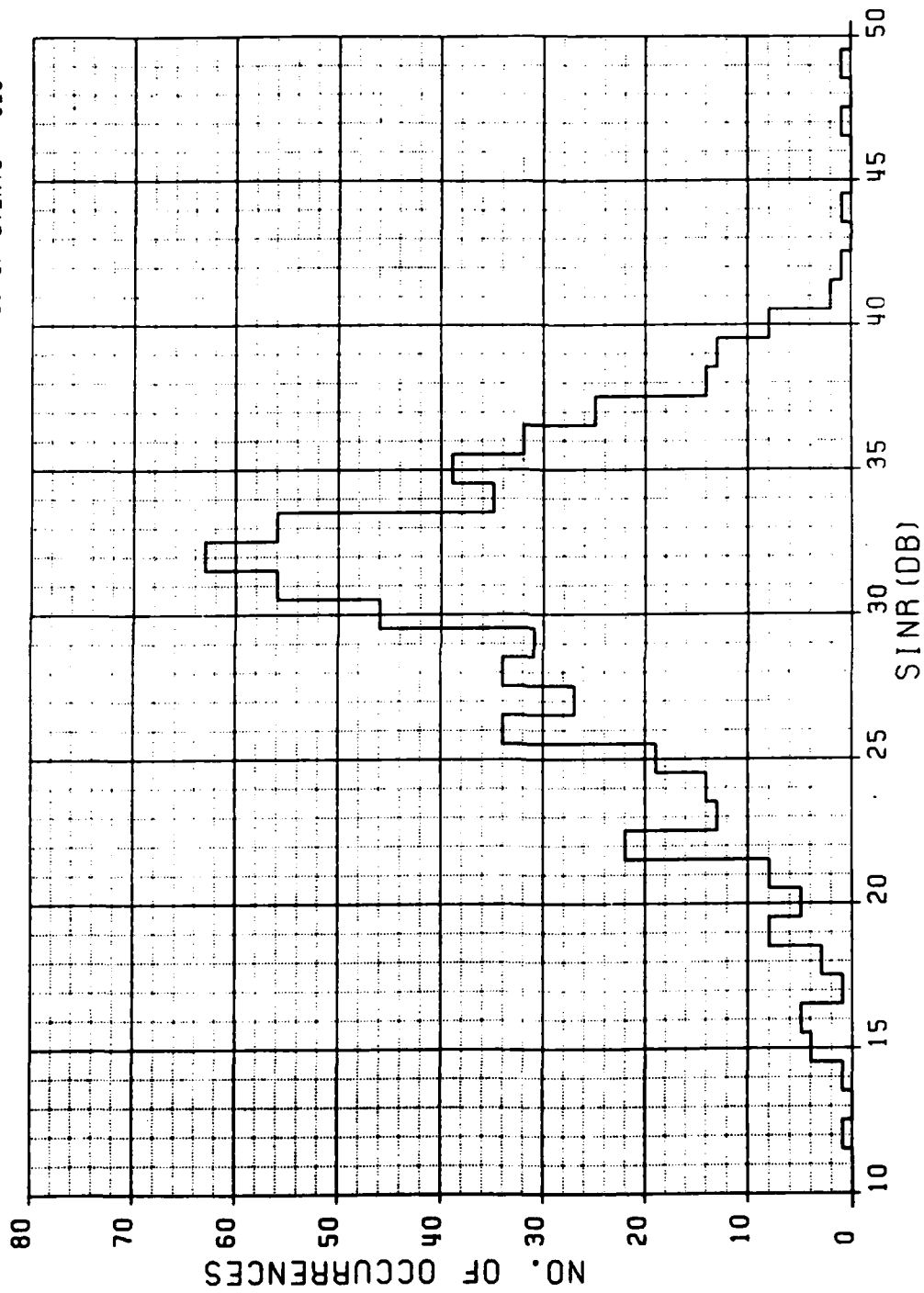NO. OF EVENTS = 623

SINR (DB)

NO. OF OCCURRENCES

Figure 18   MBA Configuration Histogram, Signal and Jammers Fading, S=0.8 .

respectively. The jamming scenario consisted of two 20 dB
jammers located at zero degrees elevation and 0.150 and 0.600
degrees azimuth. The noise floor variance was set at -7 dB.

Although the number of adaptive control loop for both the
MBA and the TPAA configurations is sixteen, the MBA
configuration was found to do quite poorly in attempting to
null more than two jammers in the same line jamming scenario
described in Section 4.3.1. The problem is believed to be
caused by the regular geometry of the MBA horn assembly which
limits the number of degrees of freedom available in directions
perpendicular to lines formed by the horns to 4. The problem
is worst for the line jamming scenario used in this study, but
is expected to be less severe for jammers located at other
non-perpendicular angular directions. Thus in order to get
some reasonable SINR values for this analysis, the number of
jammers was reduced to 2 for the MBA case as compared to the
twelve jammers used in the TPAA case.

These MBA histograms show that fading causes dispersion in
the SINR from its nonfading nominal value of 32.88 dB much like
that shown in the TPAA histograms of Figures 11 and 12. The
SINR histogram for the MBA case shows more dispersion than the
TPAA case, but still exhibits the same tendency to improve SINR
as well as degrade SINR although the latter is not as
predominant as in the TPAA case.

Figure 19 shows the loss distribution curves for the MBA
configuration for stress values ranging from 0.005 to 0.8. The
SINR loss at S=0.005 is larger than that of the TPAA case,
however, the additional loss due to spatial decorrelation
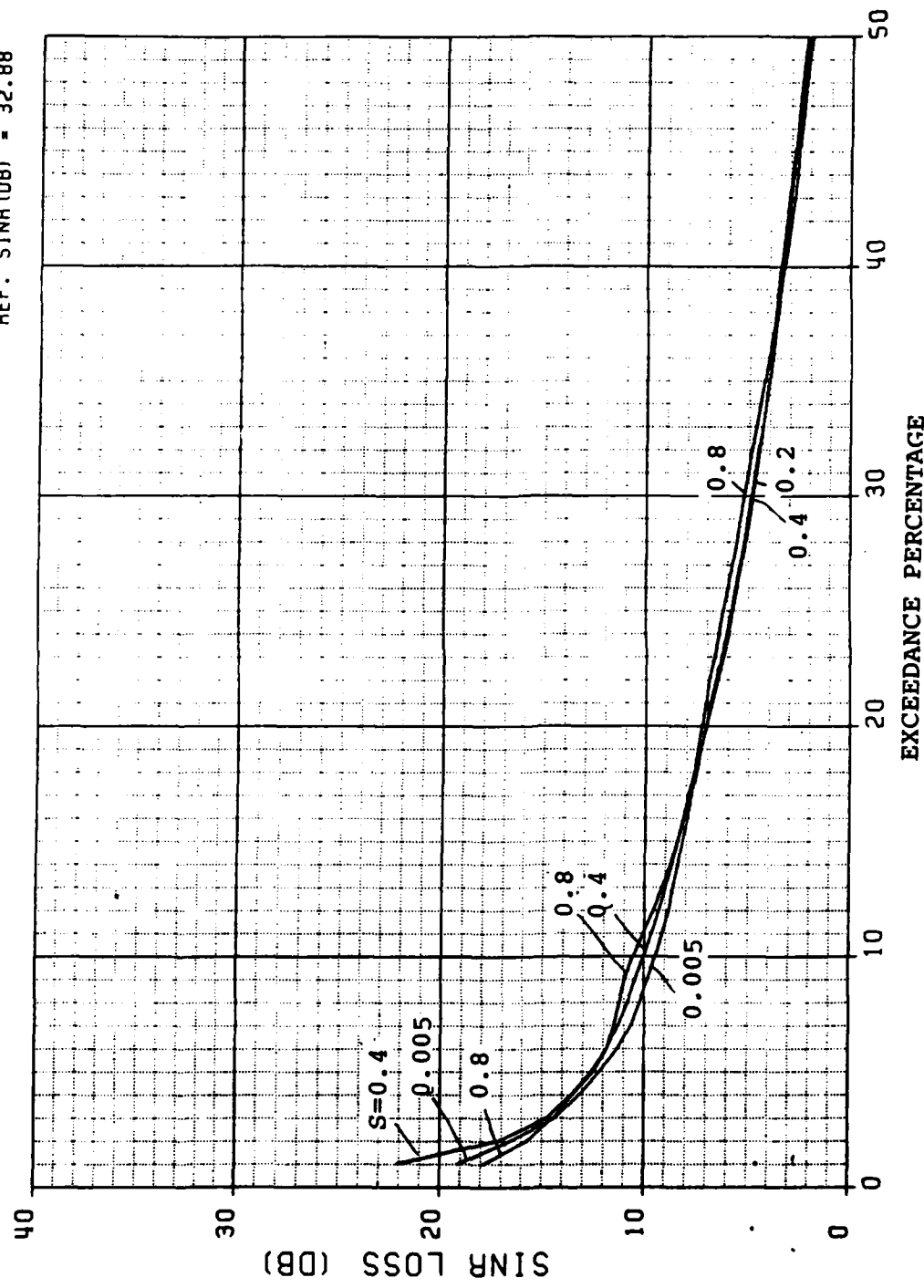distortion at higher stress values is not evident in the MBA

38

Figure 19. MBA Configuration Loss Distribution, Signal and Jammers Fading.

case as it was for the TPAA case. The relative insensitivity
of the MBA SINR loss to stress level may be partially due to
the broad area coverage beamwidth of the MBA about the desired
signal direction assumed to be at its center, the wider
beamwidth of the MBA nulls which can cover wider
angles-of-arrival with a single null, and the availability of
more unused degrees of freedom to form nulls for significant
scattered energy arriving from angles-of-arrival off the
perpendicular axes of the MBA horn configuration.

4.3.4   MBA Configuration - Jammers Fading, Signal Not Fading

The alternate fading scenario case where only the jamming
signals are affected by the fading while the desired signal is
not fading was also considered for the MBA configuration.
Figures 20 and 21 show the histograms of SINR values for
channel stress values of 0.005 and 0.8, respectively. The
jammers fading only histograms for the MBA case like the TPAA
case show a dispersion in SINR which tends toward an SINR gain
instead of a loss. Again, this occurrence is a result of the
temporal amplitude level fluctuations due to fading jammers
rather than the effect of phase decorrelation across the
aperture.

Figure 22 shows the corresponding loss distribution curves
for the MBA configuration for stress levels ranging from 0.005
to 0.8. The curves show decorrelation distortion losses
ranging from 1.5 dB at a 20 percent exceedance level to about 5
dB at a 2 percent exceedance level. As strange as it may seem,
the occurrence of signal fading appears to either exactly
cancel out the distortion loss or mask it so as to be
unnoticeable as shown in Figure 19. In any event, it appears
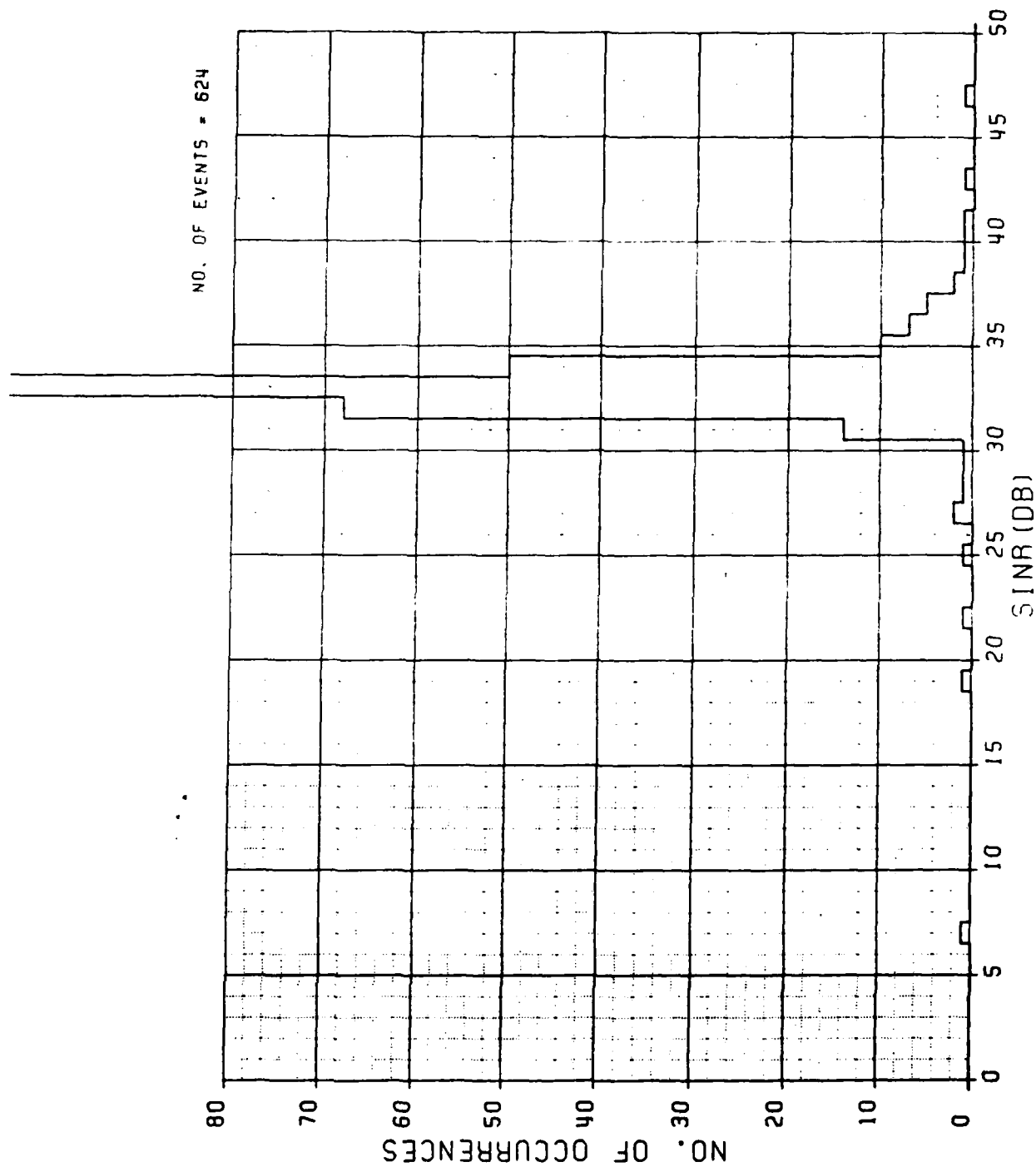
Figure 20. MBA Configuration Histogram, Jammers Fading, Signal Not Fading, S=0.005.

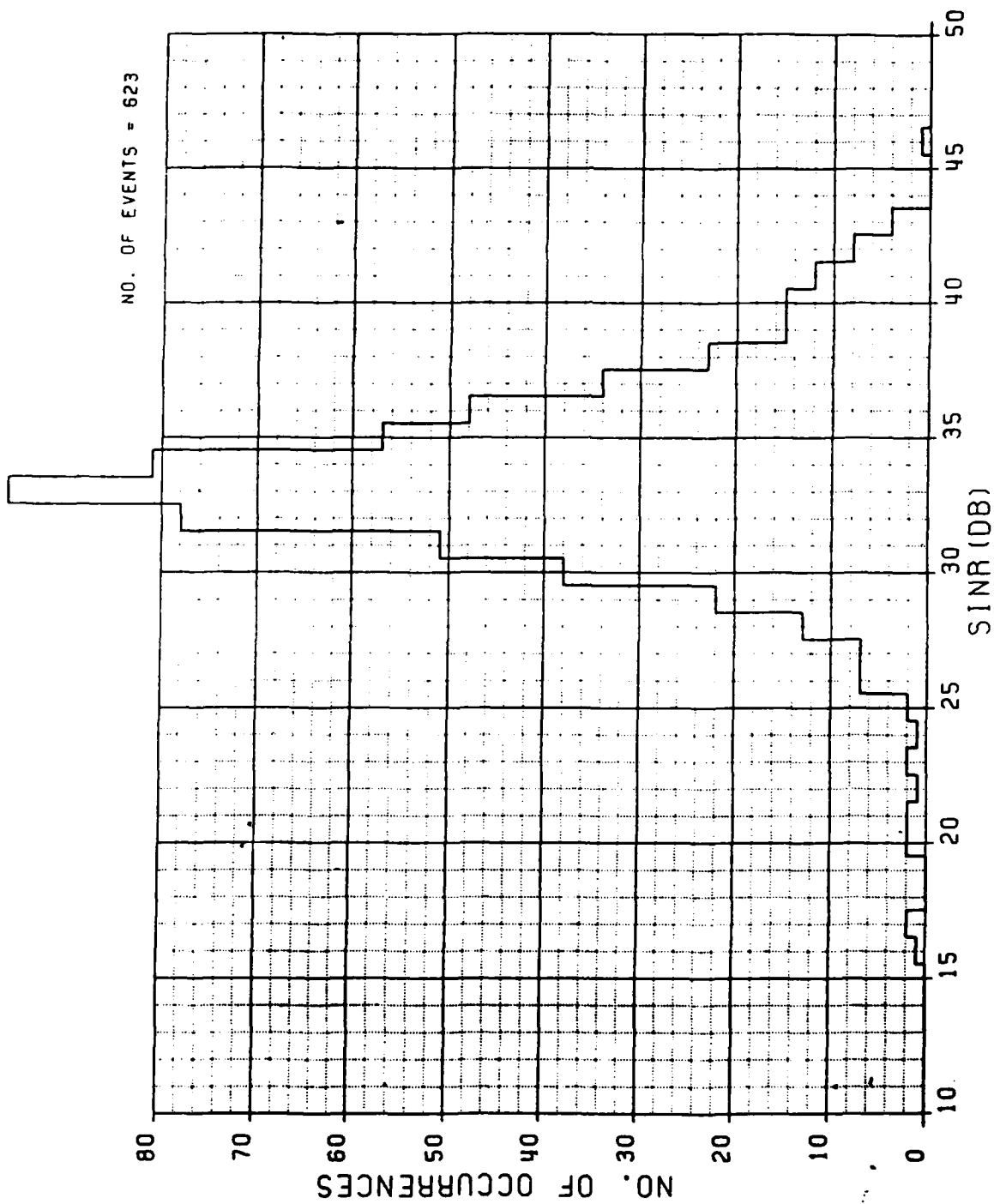NO. OF EVENTS = 623

SINR (DB)

NO. OF OCCURRENCES

Figure 21.   MBA Configuration Histogram, Jammers Fading, Signal Not Fading, S=0.8.
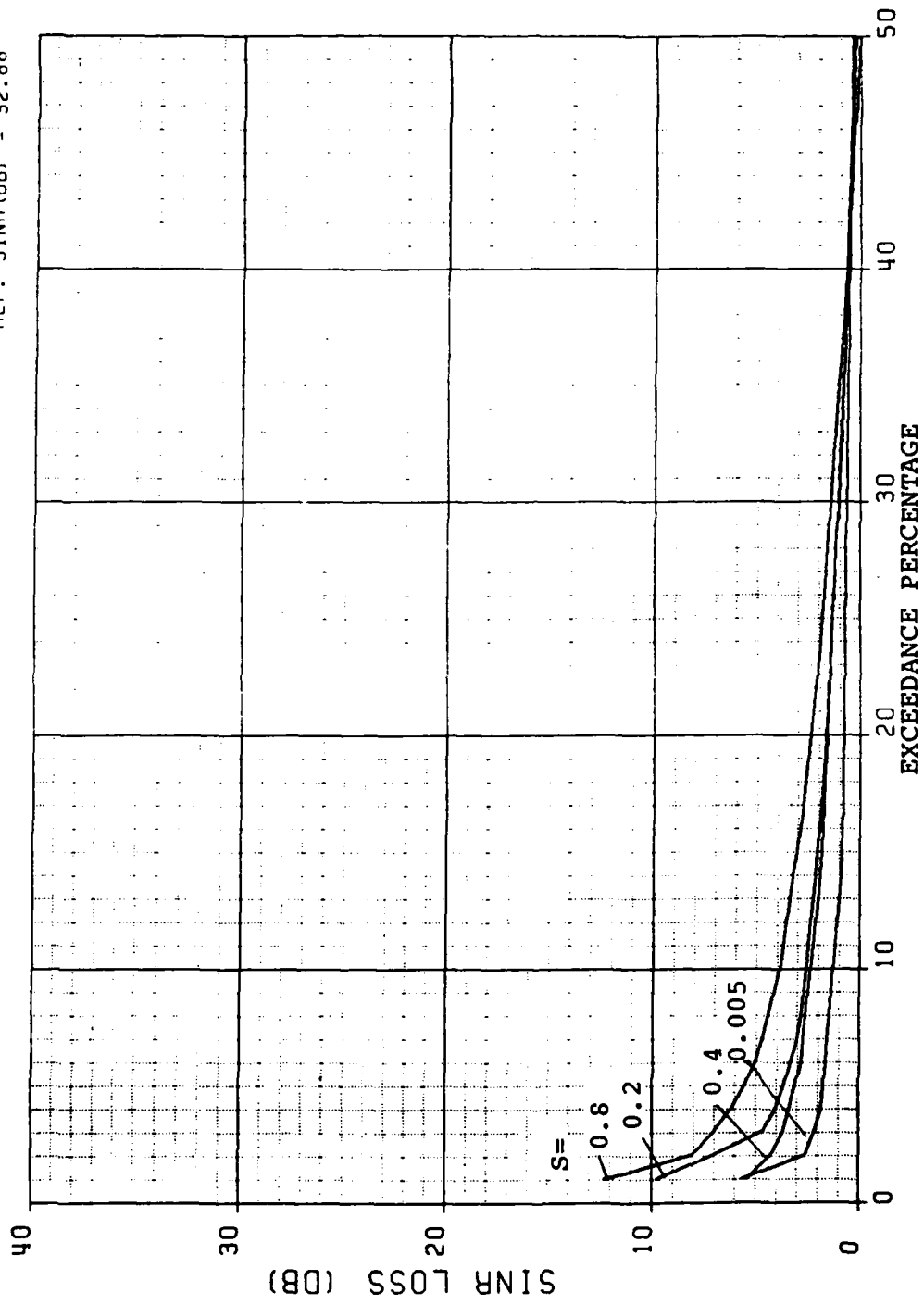
REF. SINR(DB) = 32.88

Figure 22. MBA Configuration Loss Distribution, Jammers Fading, Signal Not Fading.

43

the steady state nulling solution improves with the angularly spread jammers and non-fading signal.

4.3.5   Nonadaptive (Fixed Weights) MBA Configuration

In some applications, it may be desirable to use non-adaptively computed nulling weight based on known or computed jammer locations (by some jammer location algorithm). Since the nulling weights are not subject to real time fading corruption, it is of interest to know how the fading channel would affect these non-adaptive nulling designs.

The program which computes SINR values in fading was modified to use the ideal, non-fading nulling weights in a fading channel which identically affected the jamming and desired signals. The resulting loss distribution curves are shown in Figure 23. These results show that use of the non-adaptive nulling weights is slightly better than using the adaptive weights. A possible explanation for this result is that deep nulls are maintained in the direction each of the jammers even though the jamming levels may fade, while the unadaptive weights prevented significant desired signal power fluctuations which could occur with adaptive weights if some of the distorted jammer power appeared to come from an angular direction near that of the desired signal.
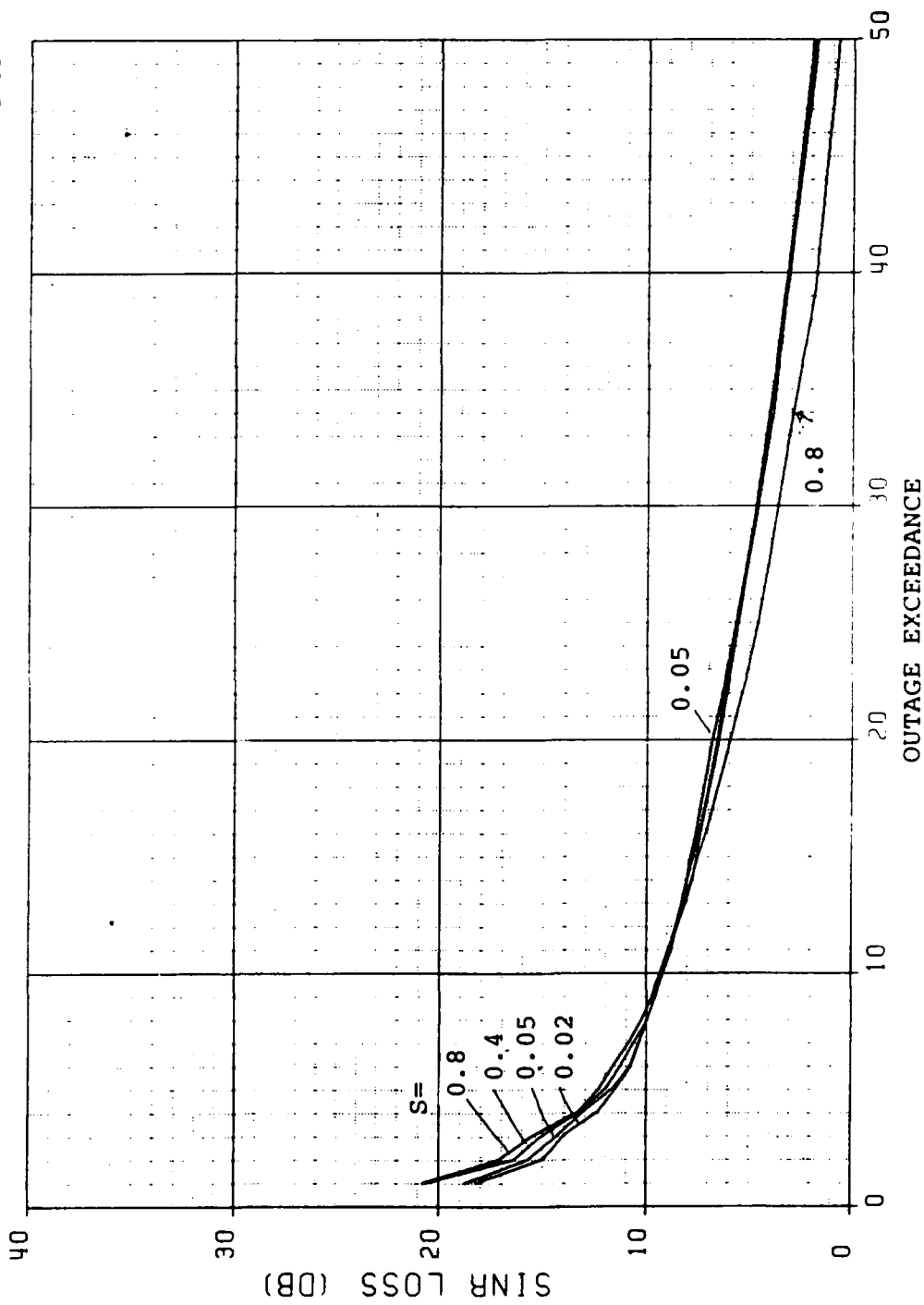
Figure 23. MBA Configuration Loss Distribution with Fixed Weights, Signal and Jammer Fading.

45

REFERENCES

1   L. Wittwer, "A Transionospheric Signal Specification for
     Satellite C^3 Applications", DNA-5662D, Defense Nuclear Agency
     Dec 1980.

2   P. Bello, "Effect of Spatial Decorrelation on Nulling
     Performance of Linear Adaptive Arrays", DNA-TR-82-170,
     Defense Nuclear Agency, 30 June 1983.

3   R. Monzingo and T. Miller, Introduction to Adaptive
     Arrays, Wiley, New York, 1980.

4   B. Widrow, et.al., "Adaptive Antenna Systems", Proc. IEEE,
     Vol. 55, No. 12, December 1967.

5   O. Frost, "An Algorithm for Linearly Constrained Adaptive
     Array Processing", Proc. IEEE, Vol. 60, No. 8,
     August 1972.

6   S. Applebaum, "Adaptive Arrays", IEEE Trans. Antennas
     and Propagation, Vol. AP-24, pp 585-598, September 1976.

7   W. Gabriel, "Introduction to Adaptive Arrays", Proc. IEEE,
     Vol. 64, No. 2, pp 239-272, February 1976.

DISTRIBUTION LIST

DEPARTMENT OF DEFENSE

Command & Control Sys Organization
    ATTN: G500, R. Crawford
    ATTN: G510, G. Jones
    ATTN: G510, P. Bird

Defense Communications Agcy
    ATTN: Code 230
    ATTN: J300, Yen-Sun Fu

Defense Comm Engineer Ctr
    ATTN: Code R123, Tech Lib
    ATTN: Code R410, N. Jones

Defense Intelligence Agcy
    ATTN: RTS-2B

Defense Nuclear Agency
    ATTN: NATF
    ATTN: NAWE
    ATTN: RAAE, P. Lunn
    ATTN: RAEE
    ATTN: STNA
3 cys ATTN: RAAE
4 cys ATTN: STTI-CA

Defense Technical Info Ctr
12 cys ATTN: DD

DEPARTMENT OF THE ARMY

US Army Communications R&D Cmd
    ATTN: DRDCO-COM-RY, W. Kesselman

US Army Information Systems Cmd
    ATTN: CC-OPS-W
    ATTN: CC-OPS-WR, H. Wilson

US Army Nuclear & Chemical Agcy
    ATTN: Library

US Army Satellite Comm Agcy
    ATTN: Doc Con

DEPARTMENT OF THE NAVY

Space & Naval Warfare Systems Cmd
    ATTN: Code 3101, T. Hughes
    ATTN: Code 501A
    ATTN: PDE-110-X1, B. Kruger
    ATTN: PDE-110-11021, G. Brunhart
    ATTN: PME 106-4, S. Kearney
    ATTN: PME 117-20
    ATTN: PME 106, F. Diederich

DEPARTMENT OF THE AIR FORCE

Air Force Weapons Laboratory
    ATTN: NTN
    ATTN: SUL

Air Force Wright Aeronautical Lab
    ATTN: A. Johnson
    ATTN: W. Hunt

DEPARTMENT OF THE AIR FORCE (Continued)

Air University Library
    ATTN: AUL-LSE

Electronic Systems Division
    ATTN: SCS-1E
    ATTN: SCS-2, G. Vinkels

Rome Air Development Center
    ATTN: OCS, V. Coyne
    ATTN: OCSA, R. Schneible
    ATTN: TSLD

Rome Air Development Center
    ATTN: EEP, J. Rasmussen
    ATTN: EEPS, P. Kossey

Space Command
    ATTN: DC, T. Long

Strategic Air Command
    ATTN: NRI/STINFO
    ATTN: SAC/SIZ
    ATTN: XPFC
    ATTN: XPFS
    ATTN: XPQ

DEPARTMENT OF DEFENSE CONTRACTORS

Aerospace Corp
    ATTN: D. Olsen
    ATTN: D. Whelan
    ATTN: I. Garfunkel
    ATTN: J. Kluck
    ATTN: J. Straus
    ATTN: K. Cho
    ATTN: R. Slaughter
    ATTN: T. Salmi
    ATTN: V. Josephson

Autometric, Inc
    ATTN: C. Lucas

BDM Corp
    ATTN: L. Jacobs
    ATTN: T. Neighbors

Charles Stark Draper Lab, Inc
    ATTN: A. Tetewski
    ATTN: D. Cox
    ATTN: J. Gilmore

Communications Satellite Corp
    ATTN: D. Fang
    ATTN: G. Hyde

EOS Technologies, Inc
    ATTN: B. Gabbard
    ATTN: W. Lelevier

Kaman Tempo
    ATTN: B. Gambill
    ATTN: DASIAC

DEPARTMENT OF DEFENSE CONTRACTORS (Continued)

Kaman Tempo
    ATTN: DASIAC

M I T Lincoln Lab
    ATTN: D. Towle
    ATTN: I. Kupiec

M/A Com Linkabit Inc
    ATTN: A. Viterbi
    ATTN: H. Van Trees
    ATTN: I. Jacobs

MAXIM Technologies, Inc
    ATTN: J. Marshall
    ATTN: R. Morganstern
2 cys ATTN: E. Tsui
2 cys ATTN: R. Ibaraki

Mission Research Corp
    ATTN: C. Lauer
    ATTN: D. Knepp
    ATTN: F. Fajen
    ATTN: F. Guigliano
    ATTN: G. McCartor
    ATTN: R. Bigoni
    ATTN: R. Bogusch
    ATTN: R. Dana
    ATTN: R. Hendrick
    ATTN: S. Gutsche
    ATTN: Tech Lib

Mitre Corp
    ATTN: A. Kymmel
    ATTN: C. Callahan

Mitre Corp
    ATTN: M. Horrocks
    ATTN: W. Foster
    ATTN: W. Hall

Pacific-Sierra Research Corp
    ATTN: H. Brode, Chairman SAGE

Pacifica Technology
    ATTN: E. Giller

DEPARTMENT OF DEFENSE CONTRACTORS (Continued)

Photometrics, Inc
    ATTN: I. Kofsky

Physical Research, Inc
    ATTN: R. Deliberis
    ATTN: T. Stephens

Physical Research, Inc
    ATTN: J. Devore
    ATTN: J. Thompson
    ATTN: K. Schlueter

R & D Associates
    ATTN: B. Moller
    ATTN: C. Greifinger
    ATTN: F. Gilmore
    ATTN: G. St Cyr
    ATTN: H. Dry
    ATTN: M. Gantsweg
    ATTN: M. Gover
    ATTN: P. Haas
    ATTN: R. Turco
    ATTN: W. Karzas
    ATTN: W. Wright

SRI International
    ATTN: A. Burns
    ATTN: C. Rind
    ATTN: D. Nielson
    ATTN: G. Price
    ATTN: G. Smith
    ATTN: J. Petriceks
    ATTN: M. Baron
    ATTN: R. Leadabrand
    ATTN: R. Livingston
    ATTN: R. Tsunoda
    ATTN: W. Chesnut
    ATTN: W. Jaye

Toyon Research Corp
    ATTN: J. Garbarino
    ATTN: J. Ise

VisiDyne, Inc
    ATTN: J. Carpenter

END

FILMED

1-86

DTIC